J. Fluid Mech. (2009), *vol.* 619, *pp.* 179–212.
doi:10.1017/S0022112008004576 Printed in the United Kingdom

The measurement of growth rates in capillary jets

H. GONZÁLEZ[1,3]† AND F. J. GARCÍA[2,3]

[1]Departamento de Física Aplicada III, Escuela Técnica Superior de Ingenieros, Universidad de Sevilla, Camino de los Descubrimientos, s/n 41092 Sevilla, Spain

[2]Departamento de Física Aplicada I, Escuela Técnica Superior de Ingeniería Informática, Universidad de Sevilla, Avenida Reina Mercedes, s/n, 41012 Sevilla, Spain

[3]Group of Electrohydrodynamics and Cohesive Granular Media, Facultad de Física, Universidad de Sevilla, Avenida Reina Mercedes, s/n, 41012 Sevilla, Spain

(Received 30 March 2008 and in revised form 10 October 2008)

The growth of perturbations on a capillary jet issuing from a circular nozzle in the Rayleigh regime is experimentally investigated. Electrohydrodynamic sinusoidal stimulation is employed to this end, along with two independent methods to obtain growth rates of the linear regime with the best accuracy so far. The first method exploits the correlation between the stimulation voltage and the breakup time measured with the help of stroboscopic images of the jet. The second method is an analysis of the spatial evolution of perturbations through a local jet-shadow-width photometry, with careful avoidance of the initial transient and the final nonlinear stages. Experiments conducted with ink allow the application of both methods, as the liquid is opaque. They give consistent results, with very small statistical errors, with respect to the expected theoretical dispersion relation, once the dynamic surface tension is adjusted. The adjusted value is in accordance with an estimate made from drop-dynamics experiments also reported here. By dealing with a simpler liquid (aqueous solution of $NaNO_3$), we are able to compare results from the first method against the theoretical predictions without adjustment of any parameter. The agreement is again excellent. Possible sources of systematic errors in this kind of measurements are identified and procedures for avoiding them are designed.

1. Introduction

The description of the instability of a capillary jet issuing from a nozzle in a gaseous ambient is a classical success of a hydrodynamic linear theory, as it is able to predict with reasonable accuracy both the breakup length of periodically perturbed jets and the size of the resulting drops. It was Rayleigh (1878, 1892) who derived the dispersion relation for this problem, using as physical model an infinitely long liquid column observed from a framework in which the column is at rest. By dispersion relation we mean, in the context of hydrodynamic stability, the dependence of the frequency with the number in a linear modal analysis of the column. In general, the frequency has a complex character that mathematically describes a wave propagation with growing or decaying amplitude. This depends on the sign of the imaginary part of the frequency, called growth rate. A detailed description of this physical model,

† Email address for correspondence: helio@us.es

usually known as temporal instability analysis, and some relevant predictions from it will be given in the next section.

The theory has been progressively refined (Eggers 1997; Eggers & Villermaux 2008). Weber (1931) considered the effect of the surrounding gas in relative motion with respect to the jet. He assumed a difference in velocity between gas and liquid at the free surface, leading to the Kelvin–Helmholtz instability. Keeping apart the influence of the outer gas, Keller *et al.* (1973) changed radically the perspective of the instability problem – a more realistic one – by means of a spatial description of the growth of perturbations, viewed from the laboratory framework: the spatial instability analysis. In the same article, they connected temporal and spatial analyses and demonstrated their equivalence in the limit of high velocity of the jet (compared to the phase velocity of capillary waves). As a consequence, the temporal approach was not given up when studying jets with such velocities. For example, Sterling & Sleicher (1975) proposed a semiempirical temporal model to account for the viscosity of the outer gas that agreed better with his experimental data than Weber's theory. Their model was experimentally tested by Kalaaji *et al.* (2003) and theoretically clarified by Gordillo & Pérez-Saborid (2005) with the help of a spatially developing boundary layer. The basic unperturbed flow is no longer translationally invariant, as the viscous stress at the free surface is different at each axial position. The consequence is the need of a redefinition of the growth rate that becomes a local parameter that eventually could be averaged throughout the linear evolution of the flow. The same difficulty arises when gravity effects are non-negligible (Cheong & Howes 2004), but no specific calculation of a correction of the Rayleigh dispersion relation has been carried out up to now.

Another possible complication in real systems is the existence of a transient region between the nozzle exit and the stream stage beyond which the velocity profile can be considered virtually flat and the jet radius uniform (Scriven & Pigford 1959; Gavis & Modan 1967). For viscous fluids the momentum diffusion is efficient enough and the transition should not extend much further than a distance of the order of the wall thickness.

Finally, for liquids with a certain amount of surfactants, the surface tension of the fresh free surface may vary considerably just in a time lapse of the order of the breakup time (Ronay 1978*a*), leading to further complications in the description of the jet dynamics. In view of that, the original idea of an infinite column sinusoidally perturbed everywhere in an non-interacting outer medium seems too simplistic, but experience has shown us that, for a certain range of jet velocities, predictions from this simple model are true with very good approximation.

Besides from experimental studies on free jets, mainly interested in the average breakup length and the dispersion in drop sizes, in the literature we find many experimental works on forced jets (Donnelly & Glaberson 1965; Goedde & Yuen 1970; Bruce 1976; Taub 1976; Pimbley & Lee 1977; Cline & Anthony 1978; Chaudhary & Maxworthy 1980; Wetsel 1980; Collicott *et al.* 1994; Chauhan *et al.* 2003; Kalaaji *et al.* 2003). Forced jets are periodically stimulated by a variety of possible means (acoustically, electrically, with a piezoelectric transductor, etc.) leading to a dominant perturbation with definite wavelength. The breakup process is highly repetitive in this case provided that the amplitude of the selected perturbation clearly stands out from noise. The growth rate corresponding to the selected wavelength is now the parameter of interest, as well as the drop characteristics (size, existence of satellites, etc.). Particularly, the measurement of growth rates allows to envisage

a quantitative comparison with the specific dispersion relation corresponding to the experimental conditions.

Among the works on forced jets mentioned above we can find some attempts to experimentally validate a dispersion relation. Two optical techniques were employed to this end: (i) stroboscopic or high-speed capture of images of a relevant portion of the jet and (ii) temporal analysis of a shadow-width photometry at specific positions in the flow, only suitable for opaque liquids (see Xing *et al.* 1996, for a thorough description). With the help of any of these techniques, these experimenters designed two different methods for measuring growth rates, namely, (i) the breakup method, which exploits a known relation between the length of the unbroken part of the flow and the initial amplitude of the induced perturbation and (ii) what we will call the amplitude-evolution method, which directly extracts the growth rate from the spatial evolution of the perturbation. Donnelly & Glaberson (1965) and Goedde & Yuen (1970) used the amplitude-evolution method from spark-illuminated photographs. Collicott *et al.* (1994) and Chauhan *et al.* (2003) followed the same procedure taking advantage of a coupled charge device (CCD) and digital fast cameras for image acquisition, respectively. Taub (1976) and more extensively Wetsel (1980) obtained growth rates through the amplitude-evolution method using the shadow-width photometry technique with the help of a laser. Bruce (1976), Pimbley & Lee (1977) and Cline & Anthony (1978) applied the breakup method to stroboscopic images of the jet. Finally, Kalaaji *et al.* (2003) implemented both the breakup method via stroboscopic images and the amplitude-evolution method through the shadow-width photometry techniques, but preferred the first method to obtain growth rates. However, due to a variety of reasons, the agreement in these previous works was not better than 5 % with respect to the theoretical predictions. The reduction of this inaccuracy and the statement of a correct measurement procedure has remained a challenge. These goals, achieved in the simplest situation, are necessary and prior to the consideration of any of the complications mentioned above (gravity, surrounding air, etc.). From a practical viewpoint, a precise determination of the growth rate has been proposed as a method of measurement of dynamic surface tension (Ronay 1978*b*; Alakoç *et al.* 2004). These are the motivations of this article. The experiments here reported belongs to the category of forced jets, with stimulation induced by electrohydrodynamic (EHD) means.

EHD stimulation was already employed by Goedde & Yuen (1970) for not very viscous fluids. They reported the application of a sinusoidal voltage to a thin electrode with a circular hole through which the jet passed. The electric pressure on the surface of the conducting liquid advectively impresses a periodic perturbation on the jet as it flows with constant velocity. This method is called 'EHD excitation' in the literature (Crowley 1983) or 'EHD stimulation' (Atten *et al.* 1995; Barbet 1997). In Crowley (1983) the essentials of EHD stimulation are characterized. Our choice of EHD stimulation is motivated by the ease of control of the perturbation amplitude. With mechanical or piezoelectric stimulation, there is neither a universal nor a simple correlation between the amplitude of stimulation and the amplitude of the jet perturbation (Chaudhary & Maxworthy 1980). Conversely, EHD stimulation guarantees a quadratic dependence between the perturbation amplitude and the applied voltage amplitude, as it will be demonstrated in § 3.5.1. A so simple correlation is convenient to the breakup method.

Two different water-based liquids have been employed in this work, namely, ink and a solution of a salt. The ink is opaque, thus it is possible to use it in the shadow-width

photometry technique, but its surface tension changes with time. Conversely, the salt solution is transparent, but its surface tension has a static known value. The experiments with the ink allows the comparison between the two methods. The second liquid provides us with an absolute validation of the applicable theory, without the adjustment of a free parameter.

The main goals of the work are: (i) to present the results of careful measurements of growth rates by the two independent methods described above; (ii) to discuss the correct selection of a theoretical model in order to compare with experimentally obtained growth rates and (iii) to show the proper use of EHD stimulation for these measurements.

In the next section, a comparison between temporal and spatial approaches is presented, as it is a central point in the interpretation of our experimental results. In § 3, the reader will find the description of the experimental setup and the methods of measurement of all relevant quantities: velocity, radius, fluid properties of the two liquids used in the experiments and growth rate. As one of the liquids – the ink – has a dynamic surface tension, a drop-dynamics technique for an estimation of this parameter is also reported in the same section. Concerning the measurement of growth rates, a detailed analysis of the breakup method and the amplitude-evolution method is carried out. The role of the electrical shielding in EHD stimulation is analysed as well. Results of growth rate measurements for an ink jet by the two methods and for the aqueous-solution jet by only the breakup method are presented in § 4. Other relevant results extracted by us from previous literature are also reported. The agreement between the growth rates obtained from each technique, as well as with the appropriate theoretical model, is discussed in § 5. Finally, the main conclusions are drawn.

2. Temporal versus spatial theory

Let us first consider the problem of a jet not influenced by the surrounding gas, in the absence of gravity. The physical properties of the liquid necessary to describe this system are the density ρ, the dynamic viscosity μ and the surface tension γ. Rayleigh's approach (Rayleigh 1892) to the capillary instability was to consider a portion of the jet as a part of an infinitely long column with radius that of the jet, R, at rest in a frame moving itself with the jet velocity v. The column shape is perturbed along its infinite extent as described in cylindrical coordinates by

$$f(z, \phi, t) = \mathrm{Re}\{f_m \exp[\mathrm{i}\,(kz - \Omega t + m\phi)]\}, \tag{2.1}$$

i.e. a sinusoidal wave with wavenumber k. Here, the non-negative integer m is usually called the azimuthal number. Ω is allowed to be complex ($\Omega = \Omega_{\mathrm{Re}} + \mathrm{i}\Omega_{\mathrm{Im}}$), with Ω_{Im} the previously referred growth rate. Accordingly, the amplitude of the perturbation evolves in time, leading to a damping for $\Omega_{\mathrm{Im}} < 0$ (stability) or a growth for $\Omega_{\mathrm{Im}} > 0$ (instability), with a subsequent breakup into drops in the last case. As mentioned, this approach is called temporal stability analysis. It could also be considered as a local theory, in the sense that it is sustained by the observation of a portion of the jet of length $\lambda_t \equiv 2\pi/k$, which we shall call temporal wavelength, and does not pay attention to what happens upstream and downstream.

We remit the reader to a careful revision of the temporal analysis carried out in García & González (2008), which includes the description of capillary and hydrodynamic modes. Two parameters are usually defined to describe the behaviour

of capillary jets in this approach, namely, the capillary time

$$t_c \equiv \sqrt{\frac{\rho R^3}{\gamma}},$$

which is the typical time scale for the evolution of the jet, and the Ohnesorge number

$$C \equiv \frac{\mu}{\sqrt{\rho \gamma R}},$$

interpreted as the ratio of viscous to capillary forces. Once the analysis is done, the sinusoidal wave perturbation is found to be unstable only for $m = 0$ and $kR < 1$, independently of the viscosity of the liquid. This case is also characterized by the absence of oscillations ($\Omega_{\mathrm{Re}} = 0$) and, consequently, a zero phase velocity Ω_{Re}/k, i.e. the observer sees a simple growth of the amplitude, without propagation. From this result, in principle another observer in the laboratory frame could measure the jet velocity by means of the velocity of a crest. The same observer could also extract the temporal growth rate from the amplitudes and positions of the crests at a given time by means of a linear correlation between the positions of the maxima and the time required by the flow to reach them: if z_n is the axial position of the nth crest, the corresponding time is $t_n = z_n/v$, and the amplitude is predicted by $f_n = f_0 \exp(\Omega_{\mathrm{Im}} t_n) = f_0 \exp(\Omega_{\mathrm{Im}} z_n/v)$. In this temporal stability analysis, the stimulation plays the role of a wavelength selector: for a stimulation period T, the corresponding wavelength is $\lambda_t = vT$ and the wavenumber is $k = 2\pi/(vT)$.

We recall that $f(z, \phi, t)$, as given by (2.1), corresponds to one among a complete set of normal modes that are solutions of the evolution equations. These modes must be combined to verify the initial conditions for deformation and velocity, as described also in García & González (2008).

On the other hand, the spatial stability analysis, presented by Keller *et al.* (1973) for inviscid liquids and by Leib & Goldstein (1986) for viscous liquids, implies a more realistic point of view. The jet is not considered as an infinite column but issuing from a nozzle. The jet velocity plays now a relevant role, so it is advantageous to define a new parameter, the Weber number

$$We \equiv \frac{\rho R v^2}{\gamma},$$

which represents the squared ratio of the jet velocity to the capillary velocity R/t_c (the natural scale for velocity of propagation of capillary waves). The Reynolds number $Re = \rho v R/\mu$ is related to the previously defined non-dimensional numbers through $Re = We^{1/2}/C$, so it will not enter in our description of the system. The shape perturbation is now built as a sinusoidal wave with amplitude dependent on the axial coordinate, which is

$$f(z, \phi, t) = \mathrm{Re}\{f_m \exp[\mathrm{i}\,(\omega t - Kz - m\phi)]\}, \tag{2.2}$$

with ω real and $K = K_{\mathrm{Re}} + \mathrm{i}\,K_{\mathrm{Im}}$ complex. In this way, we are proposing that the amplitude at the stimulation position varies sinusoidally. Again, the initial-value problem should be connected to this normal-mode description. The perturbation propagates downstream with phase velocity ω/K_{Re}. When the amplitude exponentially decreases for increasing z, the perturbation is stable. Conversely, when the amplitude exponentially increases, the perturbation is unstable: a drop periodically detaches itself from the jet at a fixed position, with frequency ω. The breakup length L_b

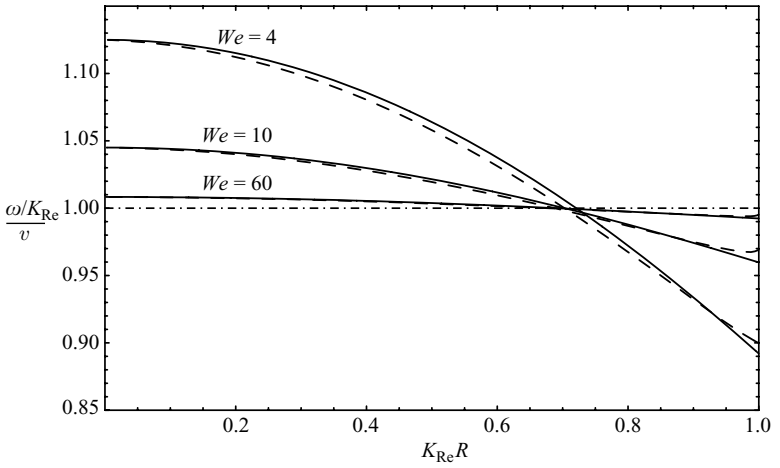

FIGURE 1. Ratio of phase velocity ω/K_{Re} to the jet velocity v as a function of the non-dimensional wavenumber $K_{\mathrm{Re}}R$, for different Weber numbers. $We = 60$ is relevant to our experiments with ink. The solid lines correspond to an inviscid liquid and the dashed line to a viscous one with $C = 0.02$, also related to these experiments. The point-dashed line shows the reference level $\omega/(K_{\mathrm{Re}}v) = 1$. Although apparent, there is no common intersection of lines with same value of C.

is the distance between that point and the position where the stimulation acts. The expected evolution observed in the laboratory frame is periodic at every jet position, with frequency ω, with the amplitude depending on the position. Again, only axisymmetric perturbations, with $K_{\mathrm{Re}}R < 1$, are unstable (i.e. $K_{\mathrm{Im}} > 0$), according to the spatial stability analysis. Note that, for the spatial description, the stimulation fixes the angular frequency $\omega = 2\pi/T$, instead of the spatial wavelength $\lambda_s \equiv 2\pi/K_{\mathrm{Re}}$ (in general different from the temporal wavelength λ_t), which is obtained from the solution $K(\omega)$ of the dispersion relation.

The spatial-instability approach is the most obvious for an experiment of a stimulated jet. In order to adopt the simpler temporal-instability approach, we must validate two assumptions:

(i) The spatial wavenumber K_{Re} coincides with that given by the temporal analysis $k = 2\pi/(vT)$. Equivalently, the phase velocity ω/K_{Re} coincides with the fluid velocity v.

(ii) The spatial growth rate K_{Im} coincides with Ω_{Im}/v.

In other words, the spatial periodicity and spatial growth are advective propagations of the temporal periodicity and temporal growth induced by the stimulation, respectively. By advective propagation we mean 'consequence of the motion of the fluid with velocity v'. The spatial analysis states that these assumptions are never strictly correct, although they are very approximate for $We \gtrsim 50$. To this respect, figure 1 helps to check the assumption $K_{\mathrm{Re}} \simeq k$ for different Weber numbers. From the figure it is also noteworthy that an observer moving with the fluid velocity v sees a capillary wave travelling downstream or upstream, depending on the wavenumber. Only one specific mode, with wavenumber slightly dependent on We and C but always in the region of maximum growth rate, does not propagate in that reference system. In contrast, in the temporal-instability approach, no propagation is predicted for any unstable mode.

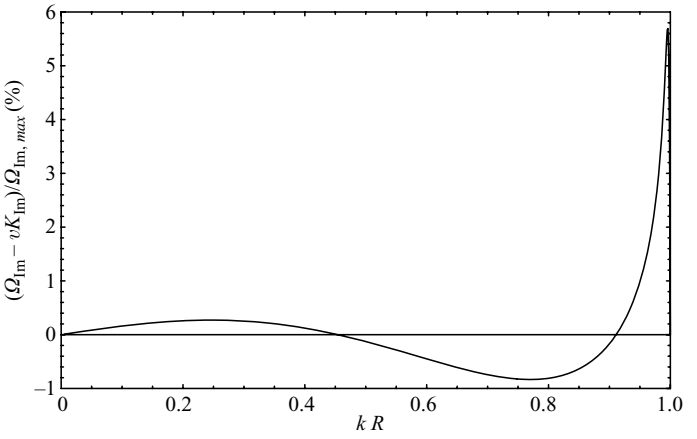

FIGURE 2. Difference between the temporal growth rate and its spatial counterpart, relative to the maximum temporal growth rate, computed from the spatial and the temporal dispersion relations, as a function of the non-dimensional wavenumber kR. The curve is calculated for values of C and We corresponding to the experiments with ink.

Under the condition $K_{\rm Re} \simeq k$, the determination of the spatial wavelength gives us a simple method to measure the velocity of the flow ($v = \lambda_s / T$). Otherwise, the relation $K_{\rm Re} = K_{\rm Re}(\omega, We) = 2\pi/\lambda_s$ still could serve us to obtain We from ω and λ_s and then to deduce the value of v from the definition of this non-dimensional number.

In relation to the assumption $K_{\rm Im} \simeq \Omega_{\rm Im}/v$, the question of how to relate the temporal growth rate with the measured quantities arises. In principle, a change to the framework where the unperturbed jet is at rest yields $\Omega_{\rm Im} = vK_{\rm Im}$. However, in general, we do not have a pure growth of the perturbation in this reference system, but also a propagation. To observe a pure growth we must change to another system with velocity equal to the phase velocity of the perturbation, leading alternatively to the relation $\Omega_{\rm Im} = (\omega/K_{\rm Re})K_{\rm Im}$. Obviously, the temporal approach is strictly valid in the limit $We \to \infty$, for which the ambiguity in this correspondence disappears. As the phase velocity is different for each wavenumber, we find more natural, following Keller *et al.* (1973), $vK_{\rm Im}$ as the quantity equivalent to $\Omega_{\rm Im}$ in the experiments.

In the context of spatial theory, plots of $K_{\rm Im}R$ versus $K_{\rm Re}R$ for different Weber and Reynolds numbers are found in figures 2–4 in Leib & Goldstein (1986), but if we are interested in the temporal approach, we find the representation $K_{\rm Im}RWe^{1/2}$ versus $\omega R/v$ more useful, as done in figure 7(*b*) in Chauhan *et al.* (2003). To give an idea of the error committed when adopting the temporal dispersion relation, under our experimental conditions, we present in figure 2 the difference $\Omega_{\rm Im} - vK_{\rm Im}$, relative to the maximum growth rate. This relative difference almost reaches 6 % very close to $kR = 1$, but remains below 1 % for $kR < 0.95$. For very precise measurements of the growth rate we are forced to use the spatial dispersion relation.

3. Experimental setup and methods

3.1. *EHD stimulation*

The system under experimental study is an electrically highly conducting liquid jet issuing vertically from a circular nozzle and surrounded by air at atmospheric pressure. The nozzle is grounded. At a short distance from the exit, between 3 and 6 mm, the jet is stimulated by a thin electrode at high-voltage placed very close to the free surface

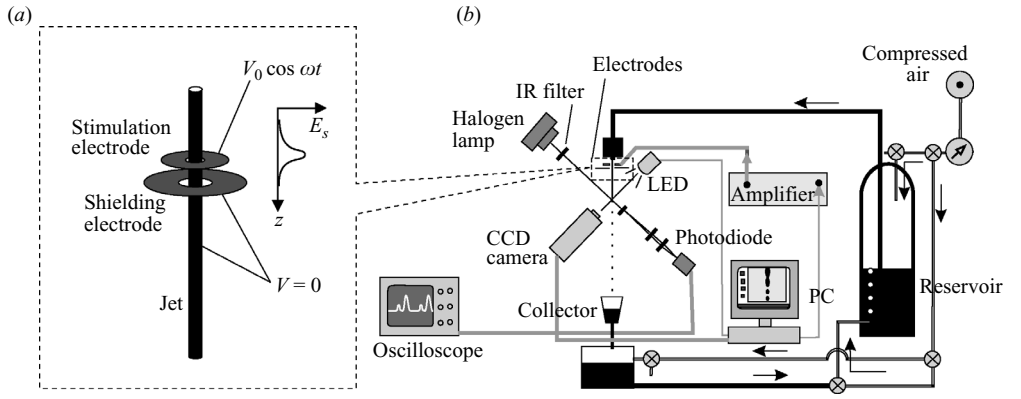

FIGURE 3. Experimental setup. (*a*) Detail of the stimulation and shielding electrodes. (*b*) General setup with the two optical acquisition techniques represented.

(see figure 3*a*). Another electrode, which is grounded, is placed below and close to the former for shielding purposes. Free charge accumulates almost instantaneously on the jet surface just in front of the electrode, where the strength of the electric field is maximum. The effect of the resulting quasi-electrostatic pressure on the jet is an EHD swelling acting very locally. The high-voltage signal is generated by means of a personal computer including a digital-analogue conversion board (Keithley DAS-1802AO) and a high-voltage amplifier (Trek 5/80). A Testpoint application digitally generates a low-voltage signal that is converted to an analogue signal and finally amplified to feed the stimulation electrode. Sinusoidal voltage signals are usually applied, but any other waveform is possible. In particular, the intermittent EHD stimulation (Hrdina & Crowley 1989) has served us to generate isolated drops with suitable deformations to estimate the dynamic surface tension of the liquid (see § 3.4.2).

Our stimulation electrode is an optical iris diaphragm made of 10 thin stainless-steel leaves, with a minimal aperture of approximately 600 μm in diameter. Another coaxial iris diaphragm, grounded and more extended, is placed parallel to the former a few millimetres below it so as to prevent the electric field from acting on a significant part of the jet. The need of this shielding is discussed in § 3.6. The jet is placed coaxially to the diaphragms due to two perpendicular micrometric screws acting horizontally. The whole system is axially symmetric, approximately. We shall also discuss the consequences of this fact in § 3.6. The device has the advantage of being retractable and easily placeable close to the jet.

3.2. *Setup*

We now turn to the remaining experimental setup (see figure 3*b*). First, we identify a hydropneumatic part responsible for the formation of the jet and the control of its velocity. The liquid comes from the bottom of a pressurized reservoir, flushes through a filter and continues towards the ejection head. A pressure regulator guarantees that the pressure of the air entering the bottom of the reservoir is constant (pressurized Mariotte bottle). Thus the velocity at the exit is constant during all the experiment, provided the ejection head does not move vertically. Notice that using an air inlet at the top of the reservoir, as in most experiments previously mentioned, would make both the pressure at the bottom and the jet velocity diminish as the liquid level lowers.

The ejection head is cylindrical, with a 236 μm in diameter circular nozzle made in a 100 μm thick stainless-steel sheet. This configuration ensures that the relaxation

length is short (less than 1 mm) after which the radial profile of velocity becomes flat (Scriven & Pigford 1959).

Verticality and positioning of the jet are achieved by appropriate mechanical actuators that supply the required degrees of freedom, linked to the ejection head. The precision in the vertical displacement is 1 μm due to a motorized translation stage.

The experimental setup is completed with two optical systems, distributed along two perpendicular horizontal optical axes. One of them gives a stroboscopic visualization of the jet. The other one implements the shadow-width technique. Here we present the basics of both.

Stroboscopic visualization consists of a CCD camera with zoom optics, aligned to both the jet and a light emitting diode (LED). The LED is fed by a pulsed electric signal of narrow width (2 μs), to have a good image definition, and with a period equal to that of the physical phenomenon to be observed. In our case this period is that of the electrostatic pressure that stimulates the jet, i.e. half the period of the voltage signal applied to the electrode. We take advantage of the *Testpoint* application to simultaneously construct stimulation and illumination signals, which are directed to two output channels: the sinusoidal signal towards the amplifier and the pulsed signal towards the LED. In this way, we bring about not only perfect synchronization, but also a precise control on the phase shift between both signals. The consequence is that the jet image is definite on the screen and we can study its evolution by incrementing the phase shift. Although the minimum step in the phase shift is 2 μs with our DA conversion board, times are measured with much higher precision. This feature is crucial in our experiment and constitutes an improvement with respect to previous works: it allows us to measure breakup times in addition to the usual measurement of breakup lengths.

In the shadow technique, a halogen source shines on the jet and merely projects its shadow, provided the liquid is opaque. The infrared part of the spectrum is previously filtered. The beam reaches a plane-convergent low-reflectance lens that projects an image amplified around 10 times on a narrow horizontal slit. In this way, a small portion in the vertical direction of the amplified beam is selected. The light passing through the slit is finally focused by a convergent lens on a photodiode. The electric signal from the photodiode is amplified and conducted to an oscilloscope (Tektronix TDS380). The DC component is not relevant and we drop it. From the remaining part we can see the temporal evolution of the jet diameter at a definite vertical position. The height of the slit (80 μm) is small compared to the diameter of the amplified image of the jet shadow, so the measurement can be considered as local in relation to the spatial evolution.

The shadow technique provides a much greater sensitiveness to detect small deformations in the jet shape. In addition, the acquisition of these data benefits from the capabilities of the oscilloscope for average calculations, which reduces the effect of hydrodynamic noise. This sensitiveness is crucial to the method because the very first stages, where the linear approximation is valid, are accessible to measurement. To this respect, our stroboscopic visualization has not enough resolution to compete with the shadow technique in analysing very small changes on the jet shape, although it could be improved with a greater optical magnification (Kowalewski 1996).

Both techniques are complementary: stroboscopy displays the spatial evolution at a fixed selectable time; shadow technique displays on the oscilloscope the temporal evolution at a fixed selectable position. They can be used simultaneously, as they are set in independent optical axes. In this way we can design measurement strategies

that benefit from the two techniques. An example is the precise measurement of the jet velocity that we report in the next subsection.

3.3. *Measurements of the velocity and radius of the jet*

Both the radius and the velocity of the jet slightly depend on the vertical position. With constant flow rate Q, their values are related through the mass preservation, which yields

$$Q = \pi R^2(z)\, v(z)$$

for the basic flow. This is why we consider their measurements together.

Two main agents may modify the velocity at each position in a jet issuing vertically: the surrounding gas and gravity. Gravity tends to increase the flow velocity. Conversely, the drag of the surrounding gas tends to reduce the velocity and makes its profile non-uniform. These effects must be estimated for our experimental conditions in order to assess the measurement of the velocity at different stages. Concerning a possible acceleration of the jet, the effect of the surrounding air is negligible since the dynamic viscosity of the gas is much less than that of the liquid and the Weber number is low (Gordillo & Pérez-Saborid 2005). Now considering the influence of gravity, for a typical velocity of 5.3 $\mathrm{m\,s^{-1}}$ the breakup length L_b is about 2 cm, which yields a relative increase $\Delta v/v \simeq g L_b/v^2$ of 0.7 % (0.9 % for $v = 4\,\mathrm{m\,s^{-1}}$), where g is the gravitational acceleration. According to (3.3), the corresponding relative reduction in radius is half of the preceding percentage. In any measurement of velocity and radius we must have in mind the existence of these variations.

In addition, we must pay attention to the consequences of moving the ejection head when visualizing different portions of the jet. Recall that, for practical reasons, the two optical axes must be fixed in the experimental setup: the jet as a whole is easier to be displaced. Every measurement (velocity and growth rates) requires vertical motions, as we shall see later. If the ejection head changes the vertical position, the jet velocity at the exit will change, according to Bernoulli's equation including gravity effects. Assuming that viscous dissipation along the hydraulic circuit is small and virtually unchanged after the motion of the ejection head, the relative reduction in the *jet velocity at the exit* v_e is estimated by $\Delta v/v_e \simeq g\Delta z/v_e^2$, with Δz the increase in the vertical position. This estimation is accurate provided the relative variation in the velocity is small. With the same condition, it is also true that the radius of the jet at the exit is fixed (Gavis & Modan 1967). According to (3.3), we thus have relative changes in the flow rate equal to those of the velocity at the exit. We have experimentally checked these changes by measuring flow rates at different positions of the ejection head and they are in excellent agreement with the expected values.

By combining the two effects described above we conclude that, as we move the position of the ejection head, the velocity at each absolute vertical position remains the same; conversely, the corresponding radius changes by virtue of the change in the flow rate. However, when regarded from the reference system of the ejection head, the radius is constant at each position but the velocity is not.

As we see, the measurement of the velocity and radius must be carefully interpreted in order to avoid systematic errors. More precisely, it is important to know at which vertical position we are making the measurement and how much we have moved the ejection head. In terms of error analysis, an inaccuracy in R propagates into the two parameters being the goal of our experiments: the non-dimensional spatial growth rate $K_{\mathrm{Im}}R$ and the non-dimensional wavenumber $K_{\mathrm{Re}}R$. In the latter parameter, the velocity is indirectly involved, as it determines the spatial wavelength λ_s and we have $K_{\mathrm{Re}} = 2\pi/\lambda_s$. The same preventions discussed for the velocity apply to λ_s. The

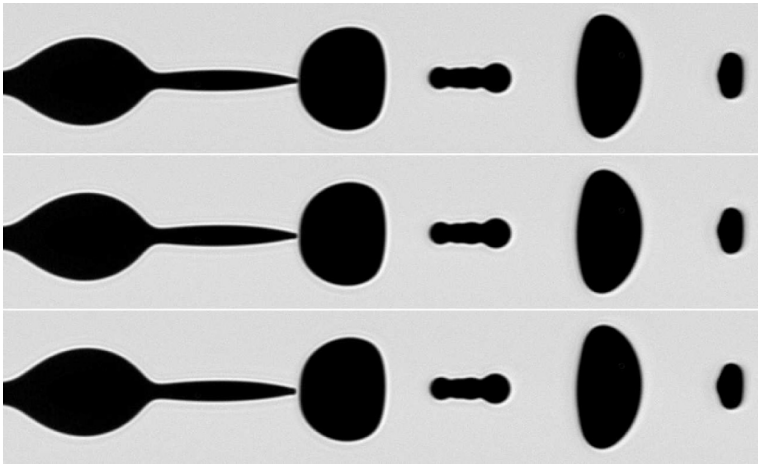

FIGURE 4. Breakup process described by three consecutive images, from top to bottom, separated 2 μs in time, among which the central one corresponds to the first detachment of a drop. The lapse between the images is the temporal resolution in the determination of the breakup time.

Ohnesorge number $C = \mu(\rho\gamma R)^{-1/2}$ and the Weber number $We = \rho R v^2/\gamma$ are also affected, but their influence on the real and imaginary parts of K, predicted by the theoretical dispersion relation, is by far less significant when C is small and We is large.

We now describe the experimental procedures and results for the measurements of the velocity and radius.

3.3.1. *Velocity*

In order to measure the velocity of the jet, most previous works have assumed that the spatial wavelength λ_s is equivalent to the temporal wavelength $\lambda_t \equiv 2\pi v/\omega$. This is also our approach, but we have been careful to avoid systematic errors. First of all, this equivalence is not accurate enough in our context of spatial instability (Keller *et al.* 1973), except for $kR \simeq 0.7$ (see figure 1). Accordingly, we select the frequency ω approximately accomplishing this condition by looking for perturbations giving the shortest breakup length, as the maximum of the dispersion relation is also near $kR \simeq 0.7$. Then we face the problem of measuring the wavelength on stroboscopic images.

The distance between consecutive main drops is more easily measured than the wavelength in the unbroken part of the flow. However, the drop velocity so obtained does not agree with the jet velocity in general (Dressler 1998). Only if $We \gg 1$, both velocities are very similar; their discrepancy can lead to misinterpretations of experimental data (Kalaaji *et al.* 2003; Attané 2006; González & García 2006).

Instead of distances between drops, we directly measure the wavelength of the perturbations in the unbroken part of the flow, by combining both the stroboscopic and the shadow techniques. To this end, we fix the phase shift between the stimulation signal and the LED signal (say zero, for instance). We then adjust the voltage amplitude until visualizing a first breakup on the computer screen (see figure 4). Progressively decreasing the voltage, we visualize the next breakup downstream. For our small stimulation amplitude, the two images are virtually indistinguishable: the only difference is an additional wavelength at the beginning of the stimulated part of

the jet for the lower-voltage case. Consequently, the difference of breakup lengths gives us the wavelength close to the stimulation electrode, even though the reference points are actually taken in the breakup region. With the only support of the stroboscopic technique, it could be measured as the displacement of the jet necessary to visualize both breakups at the same position on the screen. However, we have found the shadow technique both more precise and quick. Through comparing the stimulation signal with the LED signal, we can fix the breakup position with a precision of 1 μm, typically. As the wavelength is of the order of 1 mm, we have a relative error of 0.1 %. The precision is further increased by measuring the displacement corresponding to four or five wavelengths, which means a vertical motion of the ejection head smaller than 4 mm. This source of error is negligible when compared to those from velocity fluctuations and the above discussed gravity effects. In this way, the jet velocity is measured within a relative error of 0.2 %.

We have assumed that the periodic quasi-electrostatic force essentially constitutes a perturbation on the velocity at a given axial position, extensive to its whole cross-section. To this respect, it is important to deal with a sufficiently conducting liquid in order to avoid tangential stresses at the surface that would induce a non-uniform velocity profile.

The velocities actually measured in our experiments have ranged between 5.25 and 5.39 $\mathrm{m\,s^{-1}}$ for the experiments with ink, and values very close to 5.00, 5.96 and 7.97 $\mathrm{m\,s^{-1}}$ for the experiments with the aqueous solution of $NaNO_3$. These values are assigned to the region just after the stimulation.

3.3.2. *Radius*

In order to measure the jet radius, we initially explored a photometric technique consisting in an adaption of the shadow technique described in § 3.2 (Xing *et al.* 1996). Finally, the mass flow rate, together with the knowledge of the velocity, has given us the most precise measurement of the jet radius. The only disadvantage is being an indirect method, which makes it to inherit eventual errors in density, mass flow rate or velocity measurements. However, these three parameters are determined with very good precision in our case. Concerning the mass flow rate Q, we can reduce its error by increasing the time during which the liquid is collected until the error in Q is dominated by the error in ρ. In conclusion, the radius is obtained from $R=(Q/\pi v)^{1/2}$. The value is local and corresponds to the same position where the velocity is measured, i.e. close to the stimulation electrode. In any case, the changes in radius along the whole unbroken part of the jet have been previously estimated to be lower than 0.4 %. If we restrict ourselves to the linear part of the jet evolution, the variations are further limited.

The radii measured for the jet in the region of interest have been 108.5–108.9 μm for the experiments with ink and 108.3–109.0, 107.5–108.0 and 106.1–106.4 μm, corresponding to the three reported velocities used with the second liquid. In all cases, they give diameters smaller than that of the nozzle.

3.4. *Measurement of fluid properties*

We have used two different liquids in the experiments: ink and an aqueous solution of $NaNO_3$. The ink was mainly composed by deionized water and *n*-propanol to which a dye, containing a small amount of surfactant, is added. Evaporation during the successive runs of the experiment may change the composition. However, the mixture does not varied its physical properties very appreciably. In any case, periodic measurements have been done to have recent values of each property in a range of

temperatures which include the usual operating conditions of the experiment. The data were taken in the range 24.8 °C–27.8 °C.

The aqueous solution of $NaNO_3$ was elaborated with a 0.3 % concentration in the weight. The range of temperatures in this case was 20.9 °C–23.3 °C.

3.4.1. *Density, viscosity and conductivity*

Density was measured with five significant figures with the help of a Paar density metre DMA48. This precision is important in order to minimize errors in the determination of the radius from the flow rate. The density of the ink at the mean working temperature of 26.3 °C was $\rho = 1030.6\ \mathrm{kg\,m^{-3}}$ and had a maximum variation of $\pm 0.5\ \mathrm{kg\,m^{-3}}$ due to changes in temperature. For the aqueous solution, the density was extracted from tables (Washburn 2003). Owing to its relevance, we successfully checked those tabulated values against our own measurements. At 22.1 °C we had $\rho = 999.7\ \mathrm{kg\,m^{-3}}$ with variations of $\pm 0.3\ \mathrm{kg\,m^{-3}}$ due to changes in temperature.

The dynamic viscosity of the ink was measured using the rotating-cylinder technique with a Brookfield digital viscometer DV-II+. The corresponding value for the mean working temperature was $\mu = 1.64 \times 10^{-3}\ \mathrm{kg\,m^{-1}\,s^{-1}}$, with maximum variations of $\pm 0.06 \times 10^{-3}\ \mathrm{kg\,m^{-1}\,s^{-1}}$ due to changes in temperature. In the case of the aqueous solution, the mentioned tables give $\mu = 0.95 \times 10^{-3}\ \mathrm{kg\,m^{-1}\,s^{-1}}$ with variations of $\pm 0.03 \times 10^{-3}\ \mathrm{kg\,m^{-1}\,s^{-1}}$.

Finally, we measured the electrical conductivity of both liquids with a WTW conductivity metre LF3000, giving $1.06\ \mathrm{S\,m^{-1}}$ for the ink and $0.41\ \mathrm{S\,m^{-1}}$ for the aqueous solution.

3.4.2. *Surface tension*

Like density and viscosity, the surface tension γ of the aqueous solution is virtually that of pure water, owing to its low concentration (Washburn 2003). Measurements taken in our laboratory confirm this point and the static behaviour of this physical property. A typical value is $\gamma = 72.5\ \mathrm{mN\,m^{-1}}$ at 22 °C.

Contrarily, the determination of the surface tension of the ink requires some care. It is well known that the properties of fresh interfaces can be very different to those of the old ones, due to the influx of active substances dissolved in the bulk (Ronay 1978*a*). For our ink, the static values of γ is typically $35\ \mathrm{mN\,m^{-1}}$, as measured with a tensiometre through the Wilhelmy plate method, but if the surfactants are carefully removed, its value rises to an upper limit of $50.9\ \mathrm{mN\,m^{-1}}$. None of these values are acceptable.

The dynamic value for the surface tension should be adopted, instead of the static one, if the surface is assumed to be recent. In our case, the time of flight of the fluid particles are typically 4 ms (breakup time), to be compared to the characteristic time of influx of these molecules. As we could not know this last characteristic time, we decided to deduce the surface tension from another independent experience happening in the same time scale: we have produced isolated drops by means of pulsed EHD stimulation and studied their vibration frequency by stroboscopic visualization. This procedure was already used by Ronay (1978*b*) and Barbet (1997), but under the assumption of a linear behaviour of the drops. However, the vibration is usually nonlinear, so we have applied the numerical findings of Basaran (1992), which extends to the nonlinear regime the linear studies of Rayleigh (1879) for inviscid liquids and those of Lamb (1932) and Chandrasekhar (1961) for viscous liquids.

A voltage stimulation in the form of a square pulse (intermittent stimulation) leads to the production of one isolated main drop in the middle of the unbroken flow

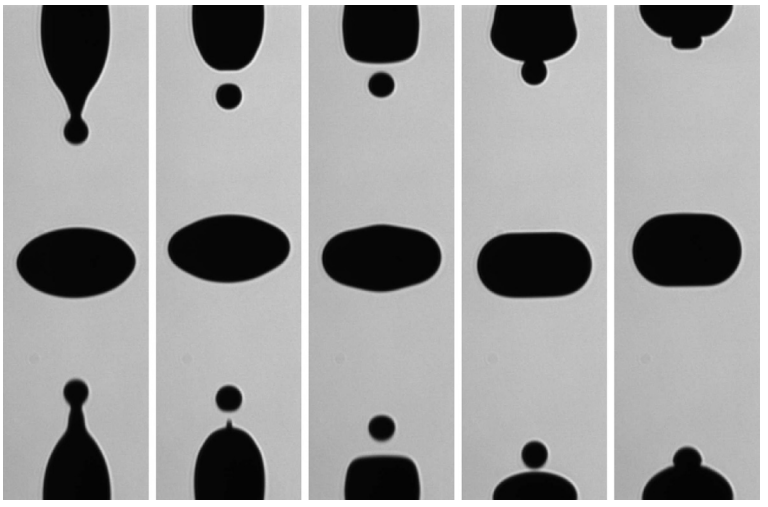

FIGURE 5. Five instants in the evolution of a jet subjected to intermittent EHD stimulation showing the region where drops have detached from the continuous flow. The main drop oscillates symmetrically with respect to the equatorial plane. The sequence proves that the satellites move away from the main drop.

(Hrdina & Crowley 1989). A train of pulses separated enough to produce independent drops allows us to visualize stroboscopically the isolated drop. Figure 5 presents a sequence of images showing the evolution of a detached main drop and its associated satellites. From it, we can observe that the satellites do not tend to merge with the main drop. This makes this generation technique very suitable for the study of isolated drops.

The phase shift between stimulation and visualization signals is controlled to analyse the drop-shape evolution with a time resolution of 2 μs. The sequence of images is digitized and processed to determine the shapes. The detachment of the main drop takes place almost simultaneously at both sides and the drop has an initial shape very deformed but almost symmetric with respect to a plane transverse to the flow. Volume and main axes are determined from the recorded shapes with high precision. A typical evolution of the ratio of polar to equatorial axes a/b is also shown in figure 6, where we can clearly observe the drop oscillation and the progressive relaxation to the spherical shape due to viscous dissipation.

We have compared oscillation periods obtained from these drop-evolution essays with numerical data from the work of Basaran (1992). In his figure 16, he plotted the change of the oscillation frequency relative to the linear-analysis prediction, for capillary Reynolds numbers $Re = 10$ and 100 (here, $Re = (R_d \gamma \rho)^{1/2}/\mu$ and R_d is the drop radius). In our experiment $Re = 67.4$, close enough to $Re = 100$ so as to take advantage of Basaran's data; even more so if we realize from the linear analysis the negligible effect of the viscosity. Another issue to be carefully considered to admit a direct comparison is the initial combination of modes in the numerical simulation. In view of the axial symmetry of the drop, the general description of a deformation reduces to

$$r(\theta) = \sum_{n=0}^{\infty} C_n P_n(\cos\theta), \tag{3.1}$$

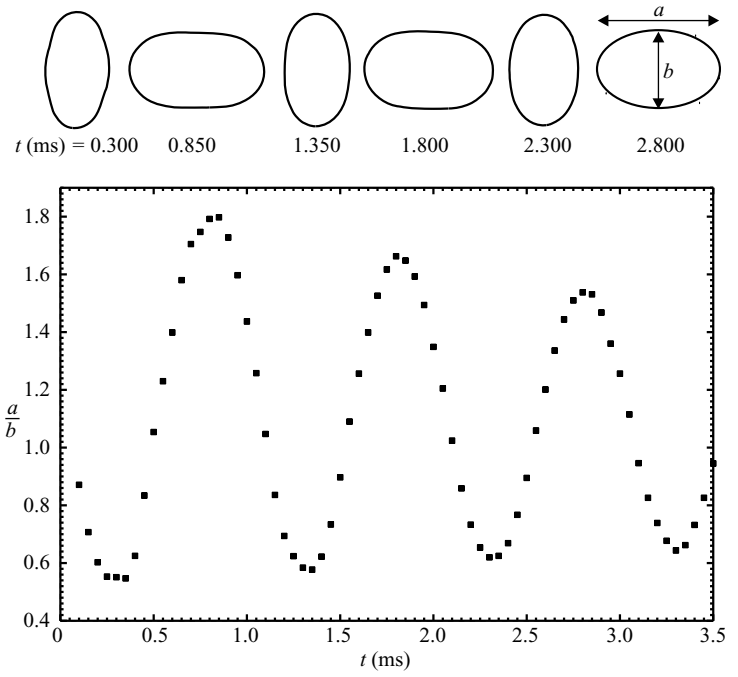

FIGURE 6. Ratio of polar to equatorial axes as a function of time in a drop detached from the main stream by means of an EHD pulse. Two complete oscillations are included. The shapes at the top of the figure are digitized images of the drop at selected times.

t (μs)	C_0	C_1	C_2	C_3	C_4	C_5	C_6	C_7	C_8
850	146.5	−0.4686	61.04	1.5560	8.242	0.6583	−0.8070	−0.0161	0.0637
1800	147.6	−0.1943	53.32	0.7557	4.924	0.3436	−0.9448	0.0238	−0.1378
2800	148.2	−0.0506	44.53	0.2297	4.309	0.0913	−0.5033	−0.0487	−0.1241

TABLE 1. First nine coefficients of the Legendre polynomials describing the shape of the isolated drop, assumed as axisymmetric, used in the determination of the dynamic surface tension of the ink. Three shapes, corresponding to the three maxima in figure 6, have been analysed.

where, as usual, $P_n(x)$ are the Legendre polynomials and θ is the polar angle in spherical coordinates. Basaran restricted his simulation to the first two even spherical modes. In our case, a modal decomposition obtained from the shape of the drops (see table 1) clearly shows that the amplitudes of modes higher than the fourth are negligible. It is also obvious that the odd modes play almost no role, as expected from our highly symmetric EHD stimulation (see figure 5). The presence of all these additional modes does not invalidate the comparison because their amplitudes are small enough to expect a negligible interaction with those selected by Basaran in his initial conditions. We have eliminated these modes to recalculate each drop shape and the corresponding ratio a/b. This procedure gives a representation of the drop evolution that slightly modifies that of figure 6. Next, we have adjusted a parabola to the set of data close to each new maximum in order to determine the oscillation periods. The comparison with Basaran's numerical simulation is then more adequate.

The surface tension obtained in this way is 52.4 $\mathrm{mN\,m^{-1}}$ from the first oscillation and 53.0 $\mathrm{mN\,m^{-1}}$ from the second, values reasonably close to the static value once the surfactants are removed. We interpret that, for our low concentrations of surfactants, the dynamic surface tension does not significantly vary during the whole evolution of the jet.

3.5. *Measurements of the growth rate*

We have measured the spatial growth rate K_{Im} in two independent ways: the *breakup method*, based on global features of the flow, and the amplitude-evolution method, giving nearly local values for K_{Im}.

3.5.1. *Breakup method*

The breakup method is based on the measurement of the breakup time or breakup length of the liquid jet for different initial amplitudes of the induced disturbance. The induced disturbance is weak. Therefore, the early evolution of the liquid jet after the stimulation is expected to be well described by the normal-mode linear analysis. As shown by García & González (2008), two normal modes are initially induced by a non-recirculating monoharmonic stimulation: a dominant mode, whose amplitude exponentially increases with time, and a subdominant mode, decreasing with time. Our initial conditions are mainly impulsive, since the liquid has no time to deform during the brief time of stimulation (García *et al.* 2000). Then both normal modes have similar initial amplitudes. Nevertheless, after an initial transient whose duration depends on the growth rates of both modes, only the dominant mode will remain, the one responsible for the growth of the deformation towards breakup. It is the initial amplitude of the dominant mode f_{d0} what we need in order to estimate the breakup length, since the subdominant mode is supposed to vanish much before the breakup.

The initial amplitude of deformation of the dominant mode, being small, is expected to be proportional to the outwards electrical pressure $(1/2)\epsilon_0 E_S^2$, where ϵ_0 is the vacuum permittivity and E_S is the modulus of the electric field in the vicinity of the jet surface. Since E_S is proportional to the amplitude of the applied voltage V_0, the initial amplitude of the dominant mode will be given by

$$f_{d0} = AV_0^2, \tag{3.2}$$

where A is a coefficient that may depend on the stimulation frequency.

If we substitute (3.2) into (2.2) with $m = 0$ we arrive at

$$f(z,t) = AV_0^2 \exp(K_{\mathrm{Im}} z)\cos(\omega t - K_{\mathrm{Re}} z), \tag{3.3}$$

where the stimulation angular frequency ω is twice the angular frequency of the stimulation voltage, owing to the quadratic relation between voltage and electrostatic pressure. If the whole evolution of the perturbation was linear, the breakup length L_b would fulfil

$$AV_0^2 \exp(K_{\mathrm{Im}} L_b) = R. \tag{3.4}$$

Although this is a simplification, it will serve us for accurately measuring the growth rate, as we discuss next. Taking logarithms in the previous expression, we arrive at

$$L_b = a - b\,\ln V_0, \quad \text{with} \quad a = \frac{1}{2K_{\mathrm{Im}}}\ln(R/A), \quad b = \frac{1}{2K_{\mathrm{Im}}}. \tag{3.5}$$

This correlation suggests measuring the breakup length for different imposed voltage amplitudes. Note that neither the unknown parameter A nor absolute values of breakup lengths are necessary to obtain the spatial growth rate K_{Im}, because it is

extracted from the slope b. Measurements of L_b relative to an arbitrary reference are enough.

Two major criticisms can be done to the use of (3.4): (i) the definition is based on (2.2), which does not take into account the transient previous to the extinction of the subdominant mode (García & González 2008) and (ii) the evolution of the jet is not linear at the breakup. For the sake of argument, we consider three zones in the unbroken flow, namely the initial linear transient part, with length denoted by L_{lt}; the central linear purely exponential part, with length L_{le} and the final nonlinear part, with length L_{nl}. Then, we may write $L_b = L_{lt} + L_{le} + L_{nl}$. Concerning each criticism separately, we state the hypothesis that both (i) the transient length L_{lt} and (ii) the nonlinear length L_{nl} are fixed for a given stimulation frequency. In this way, they do not affect the value of the parameter b defined in (3.5). The sole term dependent on the stimulation voltage is L_{le}.

These two hypothesis are crucial in the validation of the method of measurement. About the linear transient, García & González (2008) have proved that the duration of the transient depends on the growth rates of the dominant and subdominant modes, but not on any initial amplitude. There, the duration of the transient is defined as the time after which the instantaneous growth rate approaches the growth rate of the dominant mode within a prescribed maximum deviation. Simple formulae are available in that reference. L_{lt} is the duration of the transient multiplied by the jet velocity. This length accurately measures the distance from the stimulation point necessary for the subdominant mode to extinguish. We can conclude that the linear-transient length L_{lt} does not change when the stimulation amplitude varies.

Concerning the nonlinear evolution, we have verified for the ink experiments that the stroboscopic images taken at the breakup region for different stimulation strengths are virtually identical, as already mentioned in § 3.3.1. We shall later see in the same subsection that this behaviour is typical of low-amplitude stimulation, which is not always the case.

In practice, with our experimental setup, we can measure both the breakup length L_b and the breakup time t_b, i.e. the time spent by the jet since it is disturbed upstream until the first detachment of a drop downstream. We have preferred to measure t_b instead of L_b because it is both more precise and more quick. However, we must have in mind that the instability has a spatial nature. Therefore, in order to derive an expression alternative to (3.5) in terms of t_b, we should not use the evolution of the perturbation in the temporal approach (2.1) instead of its spatial approach counterpart (2.2). Rather we can employ $L_b = (\omega/K_{\mathrm{Re}})t_b$, which is strictly valid because the breakup is a consequence of the propagation of capillary waves. From this and (3.5) we find

$$t_b = c - d\,\ln V_0, \quad c = \frac{K_{\mathrm{Re}}}{2\omega K_{\mathrm{Im}}}\ln(R/A), \quad d = \frac{K_{\mathrm{Re}}}{2\omega K_{\mathrm{Im}}}. \tag{3.6}$$

As we have adopted $\Omega_{\mathrm{Im}} \simeq v K_{\mathrm{Im}}$ in § 2 as the relevant temporal quantity, from an experimentally obtained slope d we deduce $\Omega_{\mathrm{Im}} \simeq K_{\mathrm{Re}} v/(2\omega d)$. Figure 1 shows the factor $\omega/(K_{\mathrm{Re}} v)$ for different Weber numbers. For instance, in the experiments with ink ($We \simeq 60$), this factor implies a change not greater than 0.85 % to the value given by the slope, and even almost null in the region $kR \simeq 0.7$.

In order to experimentally determine Ω_{Im} for a given wavenumber, we have to measure a series of breakup times for different voltage amplitudes, as the four series with ink plotted in figure 7. For each V_0, we change the temporal phase between the stimulation signal and the stroboscopic illumination signal until visualizing the

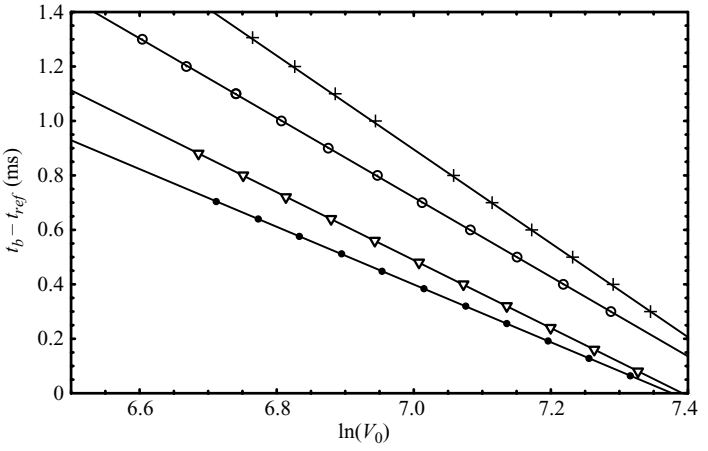

FIGURE 7. Change in breakup time relative to an arbitrary reference, as a function of the logarithm of the applied voltage amplitude in volts. Four different stimulation periods are shown, all exhibiting excellent linearity: $kR = 0.255$ (+), $kR = 0.320$ (○), $kR = 0.400$ (▽), $kR = 0.500$ (●). The spatial growth rates are obtained from the slopes.

breakup on the computer screen. That phase change gives us $t_b(V_0)$. Finally, we fit (3.6) to each experimental series of data. The temporal growth rate is inversely proportional to the slope of the linear fit. Note that we do not need the flow velocity to measure the temporal growth rate, in contrast to experiments that measured breakup lengths instead of breakup times (Goedde & Yuen 1970; Wetsel 1980; Kalaaji *et al.* 2003). As shown in figure 7, the correlation is excellent in all the series with ink. Typically we reach a Pearson coefficient of 0.99995, always over 0.9990, and even as better as 0.999999 for some essays with wavenumbers $kR \simeq 0.7$.

The linearity experimentally found is consistent with the hypothesis of $L_{lt} + L_{nl}$ constant. The results reported in § 4 have been obtained in this way.

We finally come back to the question of the invariance of the breakup region with the initial conditions. The experiments with the aqueous solution have shown slightly worse adjustments of breakup-time data to linear regressions than those with ink. Systematic deviations are detected for the highest applied voltages. This same behaviour, although much more marked, is found in the breakup-time data presented in Chaudhary & Maxworthy (1980). This work is worth to be analysed in detail, as it constitutes a very careful and documented application of the breakup technique. In figure 8, we represent their breakup time versus the voltage applied to the piezoelectric device, in logarithmic scale. It is assumed that the amplitude of the disturbance is proportional to the applied voltage. Only three representative wavenumbers are selected to discuss the effect of increasing the stimulation voltage. Each set of data should ideally fit a straight line as in our case (figure 7). Indeed, this is true in figure 8 for low-enough voltages. The lines come from a linear fit to the low-voltage data. However, we clearly observe systematic deviations from the linear fits for higher voltages. These deviations are small for $k \simeq k_{max}$, but become more evident as k differs from this value. For a given wavenumber, if we progressively discard the data corresponding to higher stimulation voltages, the remaining set fits better to a straight line. In our experiments with the aqueous solution, the stimulation with the highest voltages is almost two orders of magnitude smaller than that in Chaudhary–Maxworthy's experiments, but strong enough to observe slight systematic

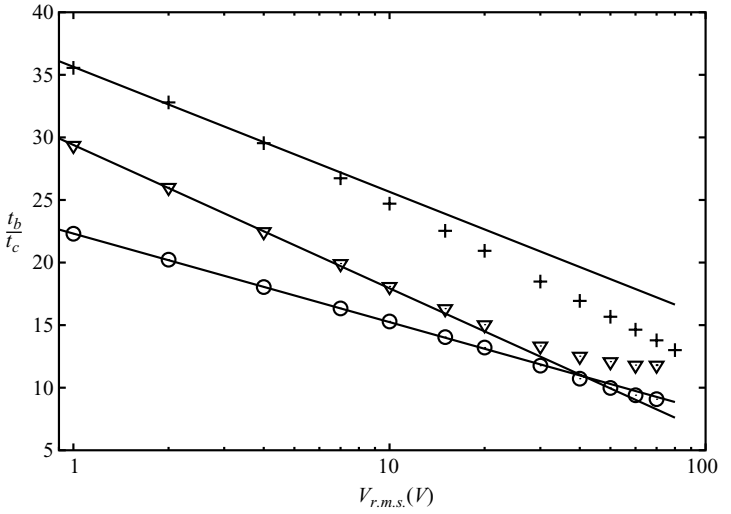

FIGURE 8. Non-dimensional breakup time t_b/t_c versus the stimulation voltage amplitude $V_{r.m.s.}$ applied to the piezoelectric device used in Chaudhary & Maxworthy (1980). Three representative wavenumbers have been selected from their original data to show different behaviours relative to linear fits: $kR = 0.31$ (+), $kR = 0.74$ (○), $kR = 0.95$ (▽). Each line corresponds to a fit of the low-voltage data.

deviations. We have avoided them through discarding the high-voltage data as described above.

3.5.2. *Amplitude-evolution method*

The amplitude-evolution method, contrary to the former, does not rely on any hypothesis about the stimulation mechanism. The spatial evolution of the jet is analysed for fixed stimulation parameters. More precisely, the shadow technique described in § 3.2 gives a periodic voltage signal whose instantaneous value is proportional to the diameter at any specific stage z in the flow. As we move downstream, the maximum axisymmetric surface deformation $f_{max}(z)$ exponentially increases according to (2.2)

$$f_{max}(z) = f_0 \exp(K_{\mathrm{Im}}\, z) \quad \Rightarrow \quad V(z) = V_{ref} \exp[K_{\mathrm{Im}}\,(z - z_{ref})], \tag{3.7}$$

where $V(z)$ is the amplitude of the AC component of the voltage recorded by the photodiode, V_{ref} is the lowest of these amplitudes in each data series and z_{ref} is the corresponding position at which V_{ref} is measured.

In the processing of the original data, a primary task is to select those data belonging to the purely exponential-growth part of the spatial evolution. Linear transients have been avoided following the criteria developed in García & González (2008). Those points corresponding to the nonlinear evolution have been discarded as well through the heuristic criterion of rejecting deformations with amplitudes greater than 10 % of the unperturbed jet radius. A theoretical analysis of systematic errors associated with this practice has not been carried out yet.

The points in figure 9 show relative voltages in logarithmic scale against the position z, obtained for perturbations with different values of kR. In accordance with (3.7), they basically follow a linear tendency in this plot. However, systematic sinusoidal deviations, usually small, are always present. An extreme case is $kR = 0.151$ (the lowest selected wavenumber). This phenomenon is not new: in figure 6 of the work of

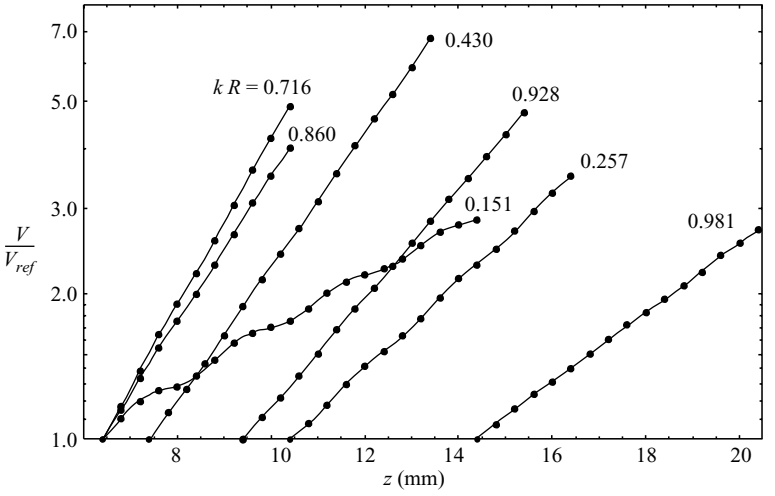

FIGURE 9. Amplitude of voltage recorded by the photodiode used in the amplitude-evolution technique, as a function of the axial position in the jet. The voltage is represented in logarithmic scale and in relative terms, using the lowest voltage of each series as the reference. Each connected set of data correspond to a stimulation frequency whose associated non-dimensional wavenumber is shown. The curves are the results of nonlinear fits described in the text.

Goedde & Yuen (1970), we observe the same behaviour. Also, Dr Atten has privately informed the authors that he has observed strong sinusoidal patterns in a conducting jet in a similar experiment with EHD stimulation, this time using a laterally placed electrode. With piezoelectric stimulation, Wetsel (1980) found a similar deviation.

Wetsel, in that work, gave a theoretical explanation for the sinusoidal deviations, based in the superposition of non-axisymmetric modes of azimuthal index $m \neq 0$ over the main axisymmetric deformation ($m = 0$). He related the presence of these modes to deviations of the exit-orifice shape from a perfect circumference. We do not enter in the validity of this guess but merely point out that other sources of non-axisymmetric modes are possible. For instance, if the ejection chamber is laterally fed, the velocity field at the exit is expected to have an axial component with an $m = 2$ mode of non-negligible amplitude. In our case, the EHD stimulation is responsible for the generation of non-axisymmetric deformations because neither the shape of the stimulating electrodes nor the electrode-jet centring are perfect. We have experimentally checked this source by deliberately placing the jet off-centre: a sinusoidal pattern appears or, if already existing, becomes more pronounced.

Wetsel claimed that, downstream, the deformation originated at the orifice evolves with a temporal angular frequency ω_m that can be estimated with the temporal approach of Rayleigh (1879) through

$$\omega_m|_{k=0} = \sqrt{m(m^2-1)}/t_c, \tag{3.8}$$

valid for an infinite column of inviscid liquid with $k = 0$. The result is a sinusoidal pattern in the axial coordinate whose wavelength is $\lambda_m = 2\pi v/\omega_m$. Wetsel's measured wavelength for the mode $m = 2$ agreed well with this formula. However, Wetsel's theoretical derivation, based on a temporal analysis, does not correctly explain either why the time-dependent deformations are detected by the photodiode or which is the role of the stimulation frequency in the generation of this $m = 2$ perturbation. A mere deformation of the orifice shape without stimulation should result in the same

spatial pattern, observed for instance in any vibrating-jet technique of measurement of the dynamic surface tension (Bohr 1909; Bechtel *et al.* 2002). However, being static, that pattern could not be detected in the spectral analysis carried out by Wetsel on his experimental data. This difficulty could be circumvented by considering that the amplitude of the radial velocity at the orifice had a sinusoidal temporal dependence that advects to any position downstream, but this last assumption is artificial because he had previously substituted $t = z/v$ at every temporal dependence in his formula in order to account for the spatial evolution.

We find more natural and rigorous the description of the non-axisymmetric pattern from a spatial analysis, using the high-velocity limit developed by Keller *et al.* (1973). Accordingly, for a given stimulation frequency ω, two waves with different wavenumbers (or, equivalently, different phase velocities) propagate downstream. They combine themselves to give a spatial pattern analogous to the acoustic phenomenon of beats occurring when two signals of unequal frequencies are simultaneously emitted. In our case, we have to think of these beats to happen in space instead of in time.

The two wavenumbers associated with the stimulation frequency ω can be expressed as

$$k_m^+ \simeq k + k_m; \qquad k_m^- \simeq k - k_m, \tag{3.9}$$

where $k = \omega/v$ is the advective propagation of the stimulation frequency ω and $k_m = \omega_m(k)/v$ is the advective propagation of the frequency $\omega_m(k)$, calculated for the mode m and wavenumber k from Rayleigh's temporal analysis. The signs plus and minus should be interpreted, respectively, as downward and upward propagation of the perturbations in a reference frame moving with the jet. These waves do not separately give a spatial pattern, but their combination does, as we demonstrate next. The general case is just a combination of both modes, each with different amplitude, say A_+ and A_-, respectively, leading to a superposition of two waves, one with spatially modulated amplitude and the other with spatially constant amplitude:

$$\begin{aligned}&\mathrm{Re}\{A_+ \exp[\mathrm{i}(\omega t - k_m^+ z)] + A_- \exp[\mathrm{i}(\omega t - k_m^- z)]\}\\ &\quad = 2\cos(k_m z)\mathrm{Re}\{A_- \exp[\mathrm{i}(\omega t - kz)]\} + \mathrm{Re}\{(A_+ - A_-)\exp[\mathrm{i}(\omega t - k_m^+ z)]\}.\end{aligned} \tag{3.10}$$

The spatially modulated wave is detected by a photodiode as a signal of frequency ω at every flow stage, but its amplitude is periodic in space with wavenumber k_m. The other term is detected as a uniform-amplitude signal.

Besides from its origin, the presence of non-axisymmetric deformations is quantitatively determined by adjusting the experimental data to a superposition of exponentials of the axial position; the sinusoidal pattern should be related to an exponential term with complex exponent. The matrix pencil method is best suited to achieve this fit (Sarkar & Pereira 1995), due to its linear nature; instead of nonlinear schemes, like the Levenberg–Marquardt algorithm, because the latter needs an initial guess which is often difficult to choose. However, the nonlinear algorithm has also been employed for testing purposes and for having an accidental-error estimate of the fit parameters. The adjusted curves in figure 9 have been generated by the matrix pencil method.

Note that the spatial analysis predicts a wavenumber related with a different natural frequency of the Rayleigh (temporal) model than that claimed by Wetsel (with $k = 0$). However, the difference is slight, as we may observe in figure 10, where a plot of the function $\omega_2(k)$ is presented and compared with data extracted from the sum-of-exponential fit. We recall that we have used the viscous temporal dispersion relation to evaluate k_m, although the change with respect to the inviscid curve is not

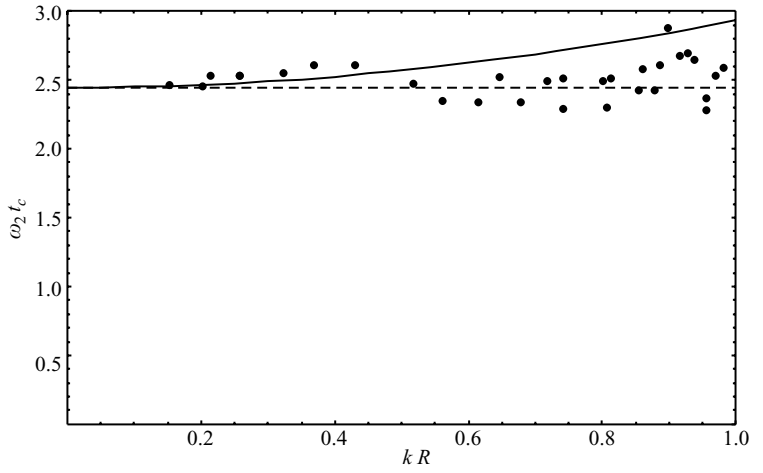

FIGURE 10. Non-dimensional frequency for the asymmetric $m = 2$ mode extracted from the data obtained by the amplitude-evolution technique, as a function of the selected wavenumber. The spatial periodicity apparent in figure 9 is related to the Rayleigh temporal analysis for that mode (see text) and the solid curve shows the theoretical prediction. The dashed line extends the value $\omega_2|_{k=0}\, t_c$ to any value of k, as proposed by Wetsel (1980).

relevant in this case. In this figure, for $kR < 0.5$, the data points are close to our proposed curve. However, the reader may find suspicious the better agreement of the experimental points having $kR > 0.5$ with the particular value of the curve at $k = 0$, as calculated by Wetsel. To this respect we must stress the fact that data with higher k are subject to higher accidental errors. The reason is apparent from figure 9, where we can observe the importance of non-axisymmetric modes for low k, in contrast to his residual character for higher k. In any case, there is no doubt about the superiority of a spatial model from the theoretical point of view.

Another issue worth to mention about the parameters obtained by the matrix pencil method is the positive character of the real part of the exponents, corresponding to growing perturbations. It is well known that the Rayleigh theory predicts damped oscillations for these modes. However, as their amplitudes are small with respect to the amplitude of the axisymmetric mode, we find this growing behaviour non-surprising, typical of slave modes that receive energy from the dominant one (Manneville 1990).

Statistical errors associated to the evaluation of Ω_{Im} are even smaller than those obtained through the breakup method. As in it, growth rates corresponding to either low wavenumbers or close to $kR = 1$ are the most difficult to obtain, due to the short range of data verifying the double restriction of being transient free and having low amplitude.

3.6. *Role of the electrical shielding in stimulation*

In previous experiments, EHD stimulation without electrical shielding gave us values of the growth rates systematically higher than expected. The reason was the destabilizing effect of a radial electric field acting on the whole jet, as shown by Melcher (1963) for a DC field applied on an inviscid fluid, by Saville (1971) for a viscous fluid and by González, García & Castellanos (2003) for a viscous fluid in an AC field. Initially, the configuration of the stimulation electrode suggested a local effect near the jet exit that should become negligible downstream. However, an estimate of the electric number $\chi = \epsilon_0 E_S^2 R/\gamma$ (with E_S the electric field on the jet

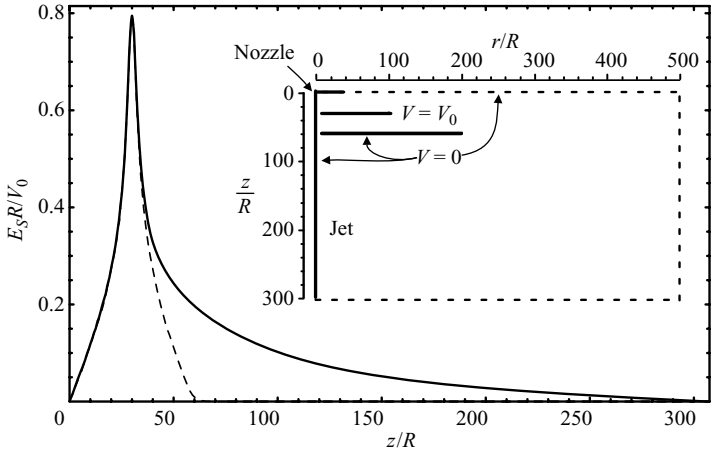

FIGURE 11. Axial distribution of electric field at the jet surface with (dashed line) and without (solid line) shielding electrode, using finite elements in the axisymmetric region represented in the attached figure. Dimensions and relative positions of both electrodes, sketched inside the main graph, are as in the experiment. The dashed line in the sketch is the closure for the computation, where we have imposed $V = 0$ as boundary condition.

surface and ϵ_0 the vacuum permittivity), which gives the relative importance of the electrostatic pressure versus the capillary-pressure jump, indicates that the influence of the electric field is not completely negligible. Indeed, the electric field on the jet computed with the help of a finite-element code gives the results shown in figure 11. From these results, the mean electric number acting on a jet 2 cm long is $\chi \simeq 0.03\, V_0^2$, where V_0 is measured in kilovolts, and typically reaches values as high as 1.3 kV. These values might be responsible for deviations in the growth rate values greater than 1 %. The effect is certainly not very important but, for a very precise determination of the growth rate, shielding is necessary. The results reported by Goedde & Yuen (1970) might be affected by the stimulation field, as the authors did not mention any shielding device in the description of their experimental setup.

Another consequence of the absence of shielding is a change in velocity due to a non-uniform electric pressure acting on the whole jet. As a matter of fact, after the passage through the stimulation electrode, the fluid particles are decelerated by the progressive reduction of the outward force exerted by the electrostatic pressure. An estimate of this acceleration is

$$\frac{\mathrm{d}v}{\mathrm{d}t} \simeq -\frac{1}{\rho}\frac{\mathrm{d}p_{inner}}{\mathrm{d}z}; \quad p_{inner}(z) = p_{outer} + \frac{\gamma}{R} - p_E(z). \tag{3.11}$$

The outer pressure and the capillary-pressure jump are essentially constant, while the electrostatic pressure is $p_E = \varepsilon_0 E_S(z)^2/2$ and $E_S(z)$ is depicted in figure 11. Integration of (3.11) between two arbitrary flow stages, z_1 and z_2, taking into account the approximate relation $\mathrm{d}t \simeq \mathrm{d}z/v$, yields a change in velocity given by

$$v(z_2) - v(z_1) \simeq -\frac{1}{\rho}\int_{z_1}^{z_2} \frac{\mathrm{d}p_E}{\mathrm{d}z}\frac{\mathrm{d}z}{v} = -\frac{\varepsilon_0[E_S(z_2)^2 - E_S(z_1)^2]}{2\rho v}. \tag{3.12}$$

For a stimulation r.m.s. voltage of some 1000 V, using the field distribution of figure 11, the relative change in velocity would be of the order of 1 %. If the determination of the wavelength was based on the stimulation frequency and on the jet velocity, the

small error in the estimate of the wavenumber would result in an important error in the assigned growth rate for the region $K_{\mathrm{Re}} \lesssim 1$. This was not the case in the experiment of Goedde & Yuen (1970), who directly measured the wavelength from photographs.

Therefore, the shielding guarantees that neither velocity, radius nor growth rate are affected by the electric stimulation.

3.7. *Summary of the experimental procedure*

Let us summarize the procedure carried out in a typical experimental essay. The liquid properties are measured previous to running the essays. For each of these, the pressure of the reservoir is fixed. We measure the jet velocity as described in § 3.3.1 by imposing a stimulation frequency leading to the shortest breakup length. Next we measure the flow rate Q and deduce the jet radius from (3.3). These steps are previous to the measurement of a series of growth rates, although the value of the velocity is often checked during the series. In each individual series we fix a stimulation frequency, measure the resulting wavelength and calculate the non-dimensional wavenumber; next, we find the corresponding growth rate by one among the two methods described in § 3.5, i.e. either we build a table of breakup times versus imposed voltage amplitudes (breakup method) or we fix the voltage and build a table of amplitudes of the oscilloscope signal versus axial positions (amplitude evolution method). From each table of data we will extract one experimental value of growth rate, corresponding to the fixed stimulation frequency. This gives one single experimental point to be compared with the theoretical dispersion relation. The procedure is repeated for different stimulation frequencies, yielding a set of experimental points, until the reservoir is empty. After recycling, we continue with the same pressure in the reservoir, or change it if we want to explore another jet velocity. In all cases, velocity and flow rate are measured again. The points shown in figures 12 and 14 are obtained in this way.

4. Results

4.1. *Ink jets*

We have measured the growth rate of ink jets with velocities close to $v = 5.3\ \mathrm{m\,s^{-1}}$ (see § 3.3.1), in a wide range of wavenumbers through both the breakup and the amplitude-evolution methods. Those results are plotted in figure 12, together with the theoretical predictions. In this section, we describe and compare the experimental data obtained with each method. The theoretical curves, calculated for $C = 0.21$ and $We = 59$, are analysed in § 5.

The growth rates presented in figure 12 have been made non-dimensional with the capillary time. We thus need the value of the surface tension. Since the value from the drop-oscillation method has an incertitude greater than the dispersion of experimental data, we have finally adopted the one from fitting our experimental data to the appropriate theoretical dispersion relation. The choice of this theoretical model is also discussed in § 5. The resulting value for the surface tension is $\gamma = 53.1\ \mathrm{mN\,m^{-1}}$.

General remarks about errors associated to growth rates obtained through the breakup method have been given in § 3.5.1. Here we merely add, in relation to figure 12, that statistical errors are greater as we move away from the region of the maximum, a fact correlated to a blurring on the stroboscopic images. The sharp images presented in figure 4 are typical of the region near k_{max}. The mentioned blurring is the obvious consequence of the ubiquitous noisy perturbations: despite of

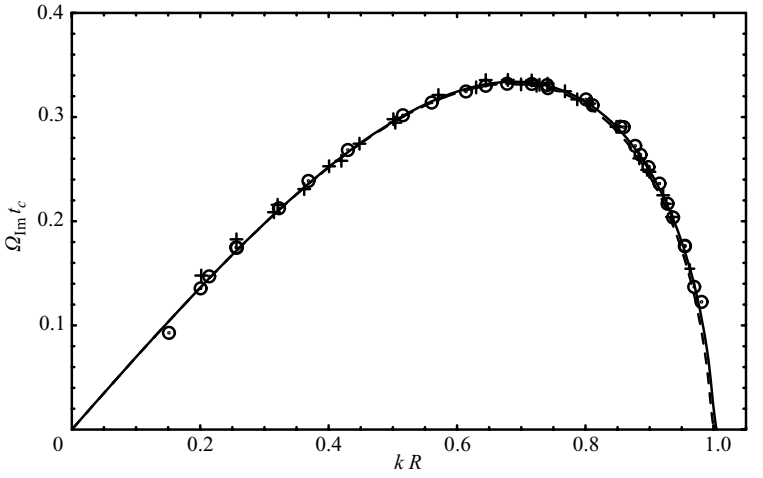

FIGURE 12. Temporal growth rate versus wavenumber, both non-dimensional, obtained from data corresponding to experiments with ink, using (*a*) the breakup time method (+) and (*b*) the amplitude-evolution method (⊙). The lines correspond to theoretical predictions with (solid line) and without (dashed line) air effect for $C = 0.021$ and $We = 59$, using the spatial analysis and a translation to the temporal variables, as discussed in § 2.

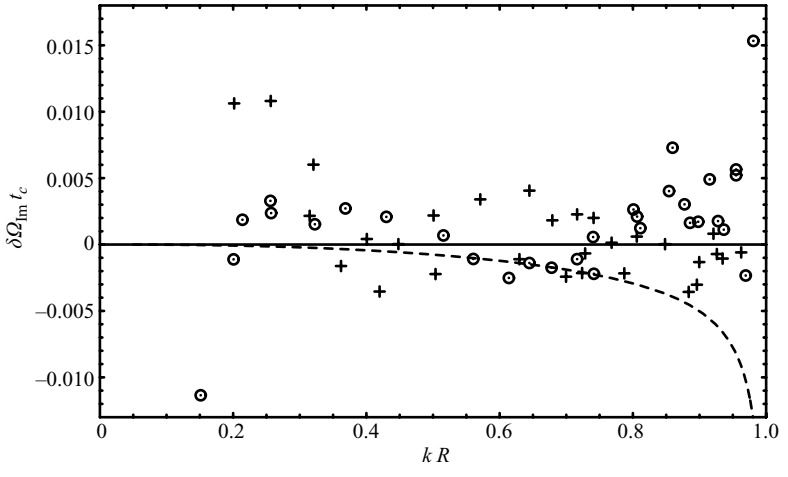

FIGURE 13. Deviations of the temporal growth rate versus wavenumber, both non-dimensional, obtained after the best fit of the theoretical curve in the case of experiments with ink. The symbols are the same as in figure 12 for each data set. The dashed line gives the difference between the growth rates calculated with the Sterling–Sleicher and Rayleigh models.

their small initial amplitude, the ones with $k \simeq k_{max}$ grow faster than the stimulated disturbance.

In figure 12 we have also represented, with a different symbol, the experimental points obtained with the amplitude-evolution method. These points have been obtained as described in § 3.5.2. Statistical errors in the growth rates are estimated as a 0.2 %, which gives an idea of how small the accidental errors are.

The accuracy of each method is analysed by calculating the deviations of the data from the theoretical curve. Figure 13 shows these deviations for both methods, each

with the same symbols as in figure 12. In fact, we have obtained the mentioned value of surface tension through minimizing the standard deviation in the range $0.35 < kR < 0.85$, for which the possible effect of systematic errors is lower. This procedure, separately employed for each data set, gives the same value of surface tension within an uncertainty of 0.05 mN m^{-1}. However, the standard deviation is lower for the amplitude-evolution method (0.0012 against 0.0017). In both cases it is small compared to the maximum non-dimensional growth rate ($\Omega_{\mathrm{Im},max} t_c \simeq 0.336$).

4.2. *Aqueous solution jets*

Ink-jet experiments have been designed with the main purpose of characterizing and comparing two independent techniques of measurement of growth rates. However, their validation through comparison with the theory is done by means of the adjustment of the surface tension of the ink. The series of experiments done with aqueous solution provides a direct comparison of one of the measurement techniques (the breakup-time one) against the theory, without adjustment of any parameter. As the liquid is now transparent, the amplitude-evolution method is not suitable in this case.

Three series of experiments, each with different jet velocity, have been carried out. They are independently presented in figure 14. The measured velocities have been reported in § 3.3.1, for which we find $We \simeq 37$, 53 and 93, respectively. Note that the central value among those Weber numbers is very similar to the one corresponding to the experiments with ink $We = 59$). The Ohnesorge number is $C \simeq 0.011$, roughly half its value in the experiments with ink. As in figure 12, the experimental data can be compared with the two theoretical curves. Deviations of almost all the experimental points are less than 1 % with respect to the curve without air effect.

Careful limitation of the stimulation voltages guaranteed a linear fit of the original data as discussed in § 3.5.1. Only the points with kR far from the maxima of the theoretical curves required voltages significantly higher than 1000 V (which is a circumstantial reference value, dependent on the particular experimental setup and different when working with ink).

4.3. *Strong stimulation in the breakup method*

In § 3.5.1 we have pointed out the risk of handling strong-stimulation data in the breakup method. In figure 15, following the procedure described in § 3.5.1 applied to the data from Chaudhary & Maxworthy (1980), we have plotted three different sets of estimates of growth rates by progressively discarding the highest stimulation voltages. In general, the agreement with the theoretical curve (computed from the original experimental parameters) improves as the fitting is restricted to smaller initial voltages. Changes mainly affect the wavenumbers far from $kR \simeq 0.7$.

5. Discussion

The first issue to be discussed will be the theoretical model applicable to our experiments. In general, jets do not exactly behave as predicted by the temporal model introduced by Rayleigh. The spatial nature of the evolution of real jets has been considered in § 1 and its relation with the temporal model has been stated in § 2. Specifically, we have made the connection between spatial quantities (ω, K_{Re} and K_{Im}) and temporal ones (k, Ω_{Re} and Ω_{Im}). The selected jet velocity in our experiments is high enough to assume small spatial effects. On one hand, we have determined the wavenumbers from the stimulation frequencies and from the independent measurement of the jet velocity near $kR = 0.7$ (see figure 1), obtaining

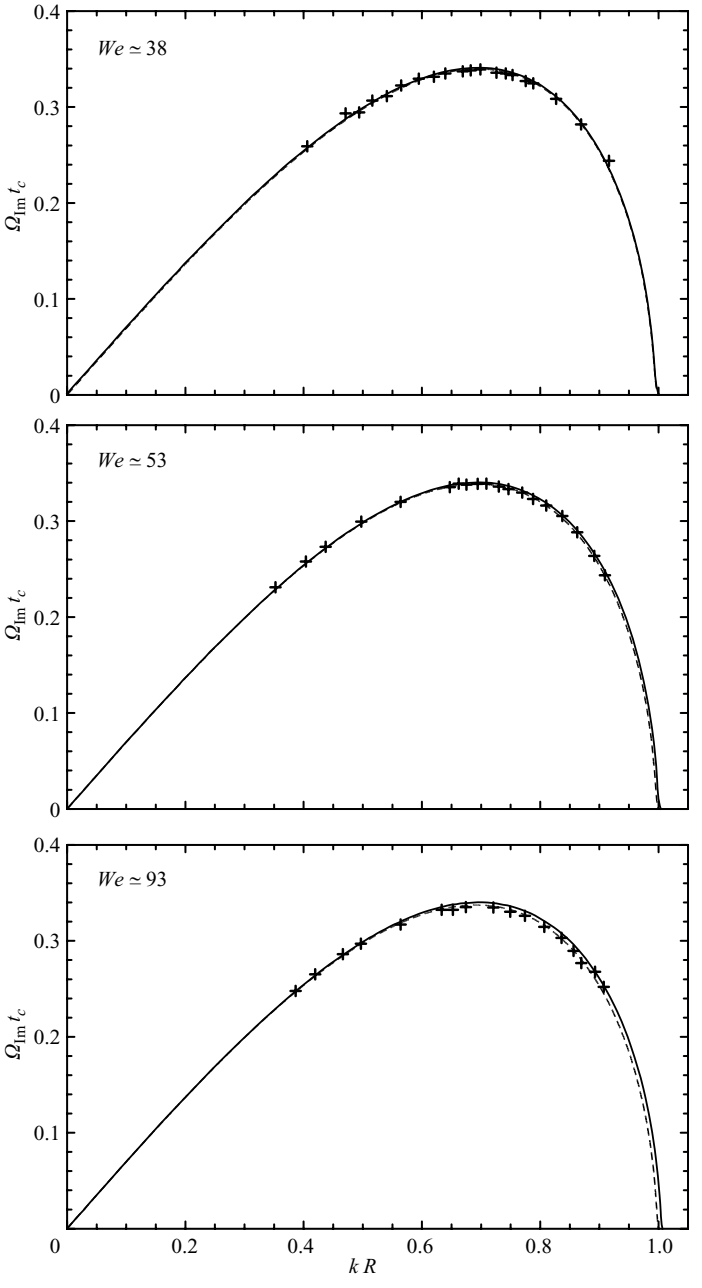

FIGURE 14. Temporal growth rate versus wavenumber, both non-dimensional, obtained from the breakup-time method for three series of experiments with the aqueous solution and with different Weber numbers. The symbols and lines mean the same as in figure 12.

in this way the temporal quantity $k = \omega/v$. On the other hand, the two methods of measurement of growth rates give values for the quantity Ω_{Im} according to the definition vK_{Im}. The curves presented in figures 12 and 13 have been computed from the spatial dispersion relation. Figure 2 gives an estimation of errors committed when disregarding spatial effects in our typical experimental conditions. These are lower

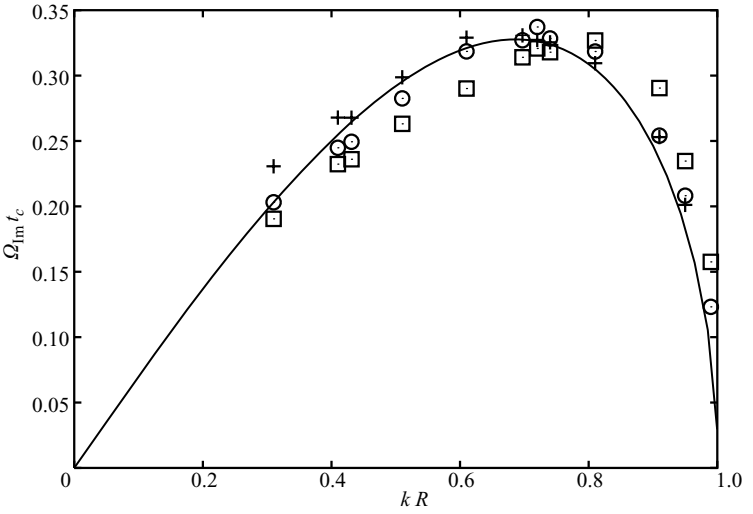

FIGURE 15. Experimental growth rate versus wavenumber, both in non-dimensional form, fitted from data of table 2 in Chaudhary & Maxworthy (1980) by selecting those data with $V_{r.m.s.} < 70$ V (□), $V_{r.m.s.} < 20$ V (⊙) and $V_{r.m.s.} < 4$ V (+). The curve represents the dispersion relation applicable to their experiment, where the stimulation frequency is fixed and the jet velocity is variable. Both spatial and aerodynamic effects are taken into account ($C = 0.0295$, from their value of t_c; $We = 19.01(kR)^{-2}$ and $\rho_a/\rho = 1.18 \times 10^{-3}$).

than 1 % except for kR very close to one, where we reach 6 %; however, the difference is hardly observable due to the sharp descent of the dispersion curve in that region, combined with the always present incertitude in the experimental values of kR. In any case, the spatial dispersion curve is as easily generated as the temporal one.

Besides from the above discussed corrections, two other effects should be taken into account: gravity effects and the action of the surrounding gas.

The effect of gravity is usually quantified through the Froude number $Fr = v^2/gL$ (L a typical length of the system), which represents the ratio of inertial forces to gravity forces; more interesting, its inverse is the relative variation of the velocity in a typical length of the system. For low velocities, this relative change before breakup is important, and so it is the change in radius by virtue of the flow rate preservation. As velocity and radius are not uniform along the jet, neither the temporal nor the spatial models are strictly applicable. In these conditions, the concept of growth rate is still useful for low variations in the jet parameters, although it becomes local (Eggers & Villermaux 2008). This local character of our measurements must make us very cautious about where we are measuring every parameter along the jet.

In our experiments, the Froude number evaluated using the breakup length ($L_b \simeq$ 2 cm) is $Fr \simeq 140$, so the effect of gravity on the whole jet is small. Moreover, for the two methods of measurement of the growth rate, the involved interval of positions has a typical length of some 6 mm, i.e. they are nearly local. The associated Froude number is $Fr \simeq 480$ and none of the complications described above ultimately affect our measurements.

The estimation made in the preceding paragraph ensures definite values for all quantities in a typical region of measurement, but we also must determine where to associate each measurement and which eventual systematic errors are induced. In § 3.3.1 we have stated that velocity and radius are measured in the region adjacent

to the stimulation zone. This also applies to the growth rate when obtained by the breakup method because the procedure is the same: a progressive reduction in the stimulation voltage that adds new portions at the beginning of the stimulated part of the jet. As a result, velocity, radius and growth rate are measured at the same region and the gravity effects do not induce any systematic error. On the other hand, the amplitude-evolution method requires data obtained beyond the transient zone, so, in general, the result does not correspond to the same region where velocity and radius have been measured. However, both regions are not very separated and the systematic errors are expected to be lower than 0.4 % for the velocity and half this value for the radius. The error in the velocity has been virtually eliminated by measuring both the growth rate and the velocity at the same absolute vertical position. This is achieved by properly selecting the range of stimulation voltages. In this way the velocity has the correct value, but the radius still differs, although very slightly, by virtue of the change in the flow rate (see § 3.3.1).

Concerning the action of the surrounding air, although the basic flow is essentially unchanged, its stability could be affected, as pointed out in § 1. For the velocities attained in our experiments, all the effects originated by the surrounding air have a small influence. In order to analyse this point, we present in figures 12 and 14 two curves: one including the air effect with the help of the Sterling–Sleicher model (solid line) and the other omitting it (dashed line) that we will call Rayleigh model although both curves come from a spatial instability analysis. The same information as in figure 12 is given in figure 13, but magnified because we deal with differences with respect to the Sterling–Sleicher predictions. In the region of maximum growth, around $kR = 0.7$, the difference is 0.6 %. For low wavenumbers, both curves become indistinguishable. For kR close to 1, although the growth rates predicted by each model are different, they are actually close from an experimental point of view, owing to the large effect of an incertitude in kR.

The sole adjusted parameter in the theoretical curves of figure 12 is the surface tension, for which we have not a very accurate value, as we mentioned in § 4. Both curves are weakly dependent on this parameter via the Weber and the Ohnesorge numbers. Simultaneously, the experimental points presented in figures 12 and 13 have been made non-dimensional using the value of the surface tension that yields the best fit. Theory and experiments present this best fit for the already mentioned value $\gamma = 53.1$ mN m^{-1}. A basic validation of both theoretical models comes from the excellent agreement between any of the two curves and the experimental data set in the whole range of tested wavenumbers. In addition, the estimated value of surface tension using the drop-dynamics technique, described in § 3.4.2, is in the range 52.4–53.0 mN m^{-1}, which is very close to the best fit value.

Further confidence in the methods of measurement and in the considered theoretical models is gained regarding the results of the series of experiments with the aqueous solution (figure 14), as in this case there is no adjustment of free parameters. The agreement is excellent for the three considered jet velocities. In addition, we are in similar experimental conditions as before: the range of selected Weber numbers includes the value corresponding to the experiments with ink and although the Ohnesorge number is different, in both cases viscous effects have small influence on the theoretical curves. We can conclude that not only the breakup method but also the amplitude-evolution method gives accurate estimations of growth rates as predicted by the theoretical models.

The experiments with the aqueous solution have explored a narrower range of values of wavenumbers than those with ink. The reason is the restriction to the

breakup method, which is less able to deal with perturbations having low growth rates.

The main observation regarding figures 12 and 14 is that the experimental data distributions are confined in narrow bands. Along with the low dispersion around the theoretical curve, our experiments improve the measurements of growth rates made up to now. To this respect, it is clarifying the review of some previous experimental data carried out by Kalaaji *et al.* (2003), comprising those of Bruce (1976), Pimbley & Lee (1977), Cline & Anthony (1978) and Chaudhary & Maxworthy (1980); some of them needed a reprocessing (appropriate non-dimensionalization and extraction of the growth rate from breakup lengths) for the sake of comparison with the dispersion relation. The work of Cline and Anthony should not be considered, strictly speaking, as a breakup-length method, because each growth rate is deduced from a sole breakup length, under the assumption of an *ad hoc* frequency-independent value of the initial amplitude. This fact, together with other irregularities in their data processing, leads us to discard their results. Among the remaining works in the previous list, the one of Chaudhary and Maxworthy (figure 15) presents the lowest dispersion in the experimental points. Even the data of Kalaaji *et al.* (2003) are not less dispersed. This is to be compared with our experiments: in the case of those conducted with ink, the points from both methods lie in a narrow band from which we may extract a $\pm 1.2\,\%$ maximum deviation for $0.35 < kR < 0.85$ and up to $\pm 3\,\%$ outside this range, except for the very extreme wavenumbers. The experiments with aqueous solution have even lower dispersion in the region of the maximum growth rate.

Beyond the coarse agreement suggested by figure 12 for the experiments with ink, some effort to discern between the Rayleigh and the Sterling–Sleicher models can be done regarding figure 13. However, clear conclusions are not expected to be drawn, owing to the small differences between both models in our experimental conditions, which are of the order of the typical dispersion of the data. Of course, we could have adopted the Rayleigh model as the basis for the estimation of the surface tension, instead of the Sterling–Sleicher one. In doing so, the overall dispersion of the data sets slightly increases and, specifically, the experimental points for $kR \simeq 1$ systematically lie above the theoretical curve. For this reason we believe that these first experiments agree better with the Sterling–Sleicher model.

The latter conclusion seems to agree with those of Kalaaji *et al.* (2003) and Gordillo & Pérez-Saborid (2005), where the Sterling–Sleicher model is tested, but we recall that these works restricted the test to modes with $kR \simeq 0.62$, i.e. in the region of the maximum growth rate. The description of how the surrounding air affects the growth rates in the whole range of unstable wavenumbers is still unaddressed. In Gordillo & Pérez-Saborid (2005), such a dispersion curve is not supplied because, as the authors demonstrated, the growth rate becomes a local concept, dependent at each axial position on the development of the boundary layer adjacent to the jet. As a consequence, the validation of the Sterling–Sleicher model cannot be quantitative and the results of a particular experiment depends on new parameters, such as the breakup length. By defining an average growth factor, specific to the experiments described in Kalaaji *et al.* (2003), Gordillo & Pérez-Saborid (2005) proposed a value for the parameter β in Sterling and Sleicher's work of 0.14, instead of the original $\beta = 0.175$. We have taken the latter to compute the solid curve in figure 12, which is the reference for the relative values presented in figure 13.

The conclusion extracted from experiments with ink contrasts with what we observe in figure 14 for the experiments with the aqueous solution. For the three Weber numbers, but especially in the case of $We = 93$, the experimental points are closer

to the Rayleigh curve than to the Sterling–Sleicher's one. The distance between the nozzle and the set of electrodes in experiments with the aqueous solution (6 mm) is significantly different from the one in experiments with ink (3 mm). According to Gordillo & Pérez-Saborid (2005), the correction due to air effect is mainly generated near the jet exit, where the boundary layer in the gas is narrow. Consequently, the actual value of β could be lower than that used in figure 14. Summarizing, although we expect the air effect to have some influence on the values of the growth rates, neither there is any theoretical curve available for fine comparison with our experimental data, nor the accuracy of the experiments in our conditions is enough to discern such a small effect.

Once the accuracy of the results has been demonstrated, the next task is to analyse the limitations of the measurement methods. Common to both of them is a progressively higher uncertainty in the measurement of growth rates for wavenumbers close to $kR = 0$ and $kR = 1$, as shown in figure 13. This is a well-known limitation motivated by the effect of natural noise in the system. If we are interested in the observation of a mode with a given wavenumber, we apply a stimulation pressure that produces a high initial amplitude of that mode. The amplitude must be high enough to hold itself, throughout the complete evolution, much greater than the amplitudes of the noisy modes; particularly, compared to those with the highest growth rate. Obviously, the modes with non-dimensional wavenumbers tending to either 0 or 1 are hardly observable as their growth rates are significantly lower than those corresponding to $kR \simeq 0.7$. This explains why the error of both methods in figure 12 is greater as we move away from the maximum. This universal limiting mechanism is the reason why we can never expect to fill experimentally the whole range $0 < kR < 1$. However, one of our goals is to describe the way to access to a wider range of wavenumbers for which the growth rates are measurable with enough precision.

There are two main risks in applying strong stimulation in order to get out from noise. First, the phase with purely exponential growth may not take a significant part of the whole process, or may even fully disappear. The consequence could be the impossibility of accurately measuring growth rates by any of both methods. This has been theoretically discussed in detail in García & González (2008).

Second, the nonlinear evolution may become dependent on the initial conditions. We must recall that the independence in the length of the nonlinear evolution with respect to initial conditions is postulated by the breakup method. Although nowadays no theoretical proof is available, Ashgriz & Mashayek (1995, figures 10–12) numerically demonstrated that large enough initial amplitudes affect both the breakup time and the sizes of satellites. Also in Chaudhary & Maxworthy (1980), we can find experimental evidence about the change in the final evolution of jets when the stimulation becomes stronger. This breaks the hypothesis about L_{nl} being independent of the initial stimulation amplitude formulated in § 3.5.1. For low voltage in the piezoelectric stimulation, the breakups have a similar form, as in our EHD stimulation, but change significantly for higher voltages. With the results presented in § 4.3, we have demonstrated the actual consequences of strong stimulation in relation to the breakup method. In figure 15, the overall agreement between theory and experiments improves when we restrict the fitting of data to weak stimulation.

On the other hand, the amplitude-evolution method is not affected by this effect when increasing the stimulation amplitude: in all the points in figure 12 corresponding to this method, the growth rates come from restricting the fits to amplitudes lower than 0.1 times the unperturbed radius, independently of the initial amplitude. Besides, the

averaging capabilities of the oscilloscope allow us to deal with weak signals, affected by noise. The range of accessible wavenumbers is greater, as shown in figure 12. In this sense, the amplitude-evolution method is superior to the breakup method. For this reason, the point with the lowest growth rates near $kR = 1$ in that figure has been obtained with the amplitude-evolution method.

6. Conclusions

The growth rates in capillary jets have been measured by means of two independent methods: the breakup-time method, based on properties of the EHD stimulation, which has been adapted from the existing breakup-length method and the amplitude-evolution method, which uses a photometric technique well tested in the literature and valid for any kind of stimulation. In the case of experiments with ink, the results from both methods are in excellent agreement and match the corresponding theoretical curve, once the dynamic surface tension is fitted. This fitted value is consistent with an independent estimate of the dynamic surface tension from the finite-amplitude natural vibration of a drop detached from the jet flow. Concerning the experiments with an aqueous solution of salt through the breakup method, the agreement is even better, with the additional advantage that no fit is needed as the surface tension is known.

The Rayleigh dispersion relation, based on a linear temporal stability analysis of the evolution of axisymmetric perturbations in a capillary jet, approximately describes the experimental data obtained in this work. For this purpose, we have selected intermediate values for the jet velocity in order to simultaneously minimize: (i) effects typical from the spatial nature of the instability, (ii) gravity effects and (iii) the action of the developing boundary layer in the gas adjacent to the free surface of the jet. The first two effects are important for low velocities and the last one for high velocities. The slight correction due to spatial effects is necessary for a more precise comparison. Gravity effects are negligible in our case. Predictions from Rayleigh and Sterling–Sleicher models are very close for our experimental conditions, and the data dispersion does not allow to discern which is the best. In any case, calculations of the air effect as those presented in Gordillo & Pérez-Saborid (2005), specific to each experiment, should be necessary for precise comparison.

Both methods of measurement of growth rates give similar results in terms of data dispersion in the range of wavenumbers for which the measurements are expected to be more precise. To this respect, the amplitude-evolution method requires the measurement region along the jet to be properly marked out: the initial transient, where the subdominant mode is non-negligible, should be discarded, as well as the nonlinear part of the evolution. The inclusion of non-axisymmetric modes in the model is also necessary for the data processing, especially for small wavenumbers.

On the other hand, the breakup-time method is sustained on the hypothesis of constant duration for both the initial transient and the final nonlinear evolution. The transient is independent of the initial amplitude, but no theoretical analysis has been done to prove that the time associated to the nonlinear evolution is independent of the initial amplitude of perturbations. However, previous numerical and experimental evidences reveal changes in the final nonlinear evolution of jets as the initial deformations become stronger. For modes with kR close to zero, the strong stimulation necessary to get them out from natural noise is a source of systematic errors for the breakup method. In any case, the ease of implementation, its

applicability to transparent liquids and its good accuracy make the breakup method a competitive way of measuring growth rates of capillary jets.

Finally, we have demonstrated the opportunity of the EHD stimulation for the design of a breakup method of measurement of growth rates, due to its clean (quadratic free of resonances) dependence with the stimulation voltage, contrary to other stimulation devices. The convenience of a shielding electrode for avoiding systematic errors in the determination of growth rates and wavenumbers has also been discussed.

We wish to thank the initial impulse given to this research by Drs Antonio Castellanos and Pierre Atten. The latter kindly has shared with us his wide experience on this subject. Josefa Guerrero has aided us in the experiments. We have benefited from the expertise in the Matrix Pencil technique of the Microwaves Group of the Departamento de Electrónica y Electromagnetismo de la Universidad de Sevilla. We are also grateful to Drs Alberto Pérez and Antonio Ramos for fruitful suggestions. This research was supported by the Spanish Ministerio de Ciencia y Tecnología under contract FIS2006-03645 and by the Junta de Andalucía under contract FQM-421.

REFERENCES

Alakoç, U., Megaridis, C. M., McNallan, M. & Wallace, D. B. 2004 Dynamic surface tension measurements with submillisecond resolution using a capillary-jet instability technique. *J. Colloid Interface Sci.* **276**, 379–391.

Ashgriz, N. & Mashayek, F. 1995 Temporal analysis of capillary jet breakup. *J. Fluid Mech.* **291**, 163–190.

Attané, P. 2006 Response to "Comment on 'Breakup length of forced liquid jet.'" *Phys. Fluids* **18**, 019102.

Atten, P., Fressard, D., Barbet, B. & Bardeau, C. 1995 Electrohydrodynamic induction of isolated drops in a jet. In *Ninth International Conference on Electrostatics, 1995, Institute of Physics Conf. Ser.* **143**, York, pp. 47–50.

Barbet, B. 1997 Stimulation Électrohydrodynamique et thermique de jets de liquide conducteur. PhD thesis, Université Joseph Fourier, Grenoble 1, France.

Basaran, O. A. 1992 Nonlinear oscillations of viscous liquid drops. *J. Fluid Mech.* **241**, 169–198.

Bechtel, S. E., Koelling, K. W., Nguyen, W. & Tan, G. 2002 A new technique for the measurement of the dynamic evolution of surface tension. *J. Colloid Interface Sci.* **245**, 142–162.

Bohr, N. 1909 Determination of the surface tension of water by the method of jet vibration. *Phil. Trans. Roy. Soc.* A **209**, 281–317.

Bruce, C. A. 1976 Dependence of ink jet dynamics on fluid characteristics. *IBM J. Res. Dev.* **1**, 258–270.

Chandrasekhar, S. 1961 *Hydrodynamic and Hydromagnetic Stability*. Clarendon.

Chaudhary, K. C. & Maxworthy, T. 1980 The nonlinear capillary instability of a liquid jet. Part 2. Experiments on jet behaviour before droplet formation. *J. Fluid Mech.* **96**, 275–298.

Chauhan, A., Maldarelly, C., Rumschitzki, D. S. & Papageorgiou, D. 2003 An experimental investigation of convective instability in a jet. *Chem. Engng Sci.* **58** (11), 2421–2432.

Cheong, B. S. & Howes, T. 2004 Capillary jet instability under the influence of gravity. *Chem. Engng Sci.* **59**, 2145–2157.

Cline, H. E. & Anthony, T. R. 1978 The effect of harmonics on the capillary instability of liquid jets. *J. Appl. Phys.* **49**, 3203–3208.

Collicott, S. H., Zhang, S. & Schneider, S. P. 1994 Quantitative liquid jet instability measurement system using asymmetric magnification and digital image processing. *Exp. Fluids* **16** (5), 345–348.

Crowley, J. M. 1983 Electrohydrodynamic droplet generators. *J. Electrost.* **14**, 121–134.

Donnelly, R. J. & Glaberson, W. 1965 Experiments on the capillary instability of a liquid jet. *Proc. Roy. Soc. Lond.* A **290**, 546–566.

Dressler, J. L. 1998 High-order azimuthal instabilities on a cylindrical liquid jet driven by temporal and spatial perturbations. *Phys. Fluids* **10** (9), 2212–2227.

Eggers, J. 1997 Nonlinear dynamics and breakup of free-surface flows. *Rev. Mod. Phys.* **69** (3), 865–929.

Eggers, J. & Villermaux, E. 2008 Physics of liquid jets. *Rep. Prog. Phys.* **71**, 1–79.

García, F. J., Castellanos, A., Atten, P. & Barbet, B. 2000 Nonlinear one-dimensional modelling of the deformation and break-up of a conducting liquid jet under intermittent EHD stimulation. In *Second International Workshop on EHD and Breakdown*, Grenoble, France, pp. 158–161.

García, F. J. & González, H. 2008 Normal-mode linear analysis and initial conditions of capillary jets. *J. Fluid Mech.* **602**, 81–117.

Gavis, J. & Modan, M. 1967 Expansion and contraction of jets of Newtonian liquids in air: effect of tube length. *Phys. Fluids* **10** (3), 487–497.

Goedde, E. F. & Yuen, M. C. 1970 Experiments on liquid jet instability. *J. Fluid Mech.* **40**, 495–511.

González, H. & García, F. J. 2006 Comment on "Breakup length of forced liquid jets" [*Phys. Fluids* 15, 2469 (2003)]. *Phys. Fluids* **18**, 1–2, 019101.

González, H., García, F. J. & Castellanos, A. 2003 Stability analysis of conducting jets under AC radial electric fields for arbitrary viscosity. *Phys. Fluids* **15** (2), 395–407.

Gordillo, J. M. & Pérez-Saborid, M. 2005 Aerodynamic effects in the break-up of liquid jets: on the first wind-induced break-up regime. *J. Fluid Mech.* **541**, 1–20.

Hrdina, D. W. & Crowley, J. M. 1989 Drop-on-demand operation of continuous jets using EHD techniques. *IEEE Trans. Ind. Appl.* **25** (4) 705–710.

Kalaaji, A., Lopez, B., Attané, P. & Soucemarianadin, A. 2003 Breakup length of forced liquid jets. *Phys. Fluids* **15** (9), 2469–2479.

Keller, J. B., Rubinow, S. I. & Tu, Y. O. 1973 Spatial instability of a jet. *Phys. Fluids* **16** (12), 2052–2055.

Kowalewski, T. A. 1996 On the separation of droplets from a liquid jet. *Fluid Dyn. Res.* **17**, 121–145.

Lamb, H. 1932 *Hydrodynamics*. Cambridge University Press.

Leib, S. J. & Goldstein, M. E. 1986 Convective and absolute instability of a viscous liquid jet. *Phys. Fluids* **29** (4), 952–954.

Manneville, P. 1990 *Dissipative Structures and Weak Turbulence*. Academic Press.

Melcher, J. R. 1963 *Field-Coupled Surface Waves*. MIT Press.

Pimbley, W. T. & Lee, H. C. 1977 Satellite droplet formation in a liquid jet. *IBM J. Res. Dev.* **21**, 21–30.

Rayleigh, L. 1878 On the instability of jets. *Proc. Lond. Math. Soc.* **10**, 4–13.

Rayleigh, L. 1879 On the capillary phenomena of jets. *Proc. R. Soc. Lond.* **29**, 71–79.

Rayleigh, L. 1892 On the instability of a cylinder of viscous liquid under capillary forces. *Philos. Mag.* **34**, 145–154.

Ronay, M. 1978*a* Determination of the dynamic surface tension of inks from the capillary instability of jets. *J. Colloid Interface Sci.* **66**, 55–67.

Ronay, M. 1978*b* Determination of the dynamic surface tension of liquids from the instability of excited capillary jets and from the oscillation frequency of drops issued from such jets. *Proc. R. Soc. Lond.* A **361**, 181–206.

Sarkar, T. K. & Pereira, O. 1995 Using the Matrix Pencil Method to estimate the parameters of a sum of complex exponentials. *IEEE Antennas Prop. Mag.* **37** (1), 48–55.

Saville, D. A. 1971 Stability of electrically charged viscous cylinders. *Phys. Fluids* **14**, 1095–1099.

Scriven, L. E. & Pigford, R. L. 1959 Fluid dynamics and diffusion calculations for laminar liquid jets. *AIChE J.* **5**, 397–402.

Sterling, A. M. & Sleicher, C. A. 1975 The instability of capillary jets. *J. Fluid Mech.* **68**, 477–495.

Taub, H. H. 1976 Investigation of nonlinear waves on liquid jets. *Phys. Fluids* **19**, 1124–1129.

Washburn, E. W. 1926–1930; 2003. *International Critical Tables of Numerical Data, Physics, Chemistry and Technology*. Knovel.

Weber, C. 1931 Zum Zerfall eines Flüssigkeitsstrahles. *Z. Angew. Math. Mech.* **11**, 136–154.

Wetsel, G. C. 1980 Capillary oscillations on liquid jets. *J. Appl. Phys.* **58**, 3586–3592.

Xing, J. H., Boguslawski, A., Soucemarianadin, A., Atten, P. & Attané, P. 1996 Experimental investigation of capillary instability: results on jet stimulated by pressure modulations. *Exp. Fluids* **20**, 302–313.